Analysis of a Cardiac Displacement Signal Recorded with an Ultrasound Vibrometer

Master Thesis
Biomedical Engineering and Informatics
Project Group: 18gr10407

AALBORG UNIVERSITY
STUDENT REPORT

Aalborg University
School of Medicine and Health
Fredrik Bajers Vej 7
DK-9220 Aalborg Øst

AALBORG UNIVERSITY
STUDENT REPORT

School of Medicine and Health
Fredrik Bajers Vej 7
DK-9220 Aalborg Ø
http://smh.aau.dk

Title:
Analysis of a Cardiac Displacement Signal Recorded with an Ultrasound Vibrometer

Theme:
Master's thesis

Project Period:
Spring Semester 2018

Project Group:
18gr10407

Participants:
Ásgerður Arna Pálsdóttir
Dagbjört Helga Eiríksdóttir

Supervisor:
Johannes Struijk

Copies: Online

Page Numbers: 61

Date of Completion:
7th of June 2018

Abstract:

Cardiac disease is the leading cause of death globally. Most cardiovascular disease can be prevented or managed with early detection. Early detection could be increased by routine monitoring where a disease could potentially be found before any symptoms appear. Traditional methods for detecting heart disease include photoplethysmography, ECG, accelerometer etc. These methods are limited by the requirement of physical contact. A promising non-contact method for detecting cardiac activity utilizes the vibrations on the surface of the body to frequency modulate a carrier ultrasound wave that can be recorded by a microphone. The goal of this project is to examine this method further.
A cardiac signal was recorded from 13 healthy subjects using an ultrasound transducer and microphone, at four distances (10 - 40 cm) with T-shirt on or off. The ultrasound (US) signal was demodulated using arctan demodulation to get the displacement of the chest wall. Continuous wavelet transformation and different filters were used to analyze different frequency bands of the US signal. The waveform of an individual heart beat from the acceleration US signal was compared with a corresponding heart beat from an accelerometer. Lastly, physiological events associated with heart valve opening and closing were transposed from the acceleration US signal to the displacement US signal.
The linking of different frequency bands with movements caused by different physiological events such as breathing and heart beats corresponded to literature in terms of frequency and amplitude (mean peak-to-peak amplitude (ppAmp), 3.5 mm and 0.3 mm, respectively). Furthermore, mean ppAmp for low frequency seismocardiographic (SCG) signals and frequency band corresponding to valve sounds was calculated (0.08 mm and 0.007 mm, respectively). The waveform correlated well with the accelerometer where the highest correlation was 0.969.
The displacement US signal contains a lot of information that has potential for being used in a clinical and out of hospital setting. Future research would include establishing physiological events on the displacement US signal along with improving the system setup.

Preface

This master's thesis in Biomedical Engineering and Informatics was performed at Aalborg University during the period 1st of February - 7th of June. In this project, a novel non-contact method for recording cardiac events was examined. Vibrations on the surface of the chest wall were used to frequency modulate a carrier wave. The signal was demodulated to get the displacement of the chest wall followed by an examination of information in different frequency bands. The wavelet of an acceleration US signal was compared with an accelerometer, and lastly physiological events were transposed from the acceleration US signal to a displacement US signal.
Sources are referenced using the Vancouver method where the sources are given in chronological order as they are used in the report. The full reference list can be found in the back of the report. References are used in the following fashion throughout the report:

- If the reference is located before a period in the end of a sentence, it refers to that particular sentence.
- If the reference is located after a period in the end of a paragraph, it refers to that paragraph.
- If a reference is referenced by first author name in the beginning of a paragraph, it refers to the rest of the paragraph unless a new reference is made.
- If a figure does not contain a reference the figure is made from data acquired in this project.

We would like to thank our supervisor from Aalborg University, Johannes Struijk for providing the project and great supervision.

Aalborg University, 7th of June 2018

Ásgerður Arna Pálsdóttir
<apalsd16@student.aau.dk>

Dagbjört Helga Eiríksdóttir
<deirik16@student.aau.dk>

Contents

Part I

Problem Specification

Chapter 1

Problem Analysis

1.1 Introduction

It is estimated that every year around 17 million people die from heart disease, making it the leading cause of death globally [1]. Most cardiovascular diseases can be prevented or managed with early detection, which is thus of great benefit, causing the treatment to be easier, more efficient and economical. Early detection could be increased by routine monitoring, i.e. measurement of human physiological parameters on a periodic check up (e.g at home), where a disease could possibly be found before any symptoms appear. A lot has been learned in the past few years about heart disease, creating a possibility for early detection. [2]

There are many methods for detecting heart disease but the most used ones are in a clinical setting, such as auscultation, photoplethysmography (PPG) and electrocardiogram (ECG). Furthermore, some sensors have been developed to detect surface vibrations such as accelerometers and laser Doppler. All of these methods provide reliable results when properly executed but are limited in some way, mostly because of the requirement for a physical contact. [3, 4, 5]

The drawbacks and limitations of the previous methods, combined with increasing possibilities in medical, research and commercial settings has led researchers worldwide to explore other ways to optimize the measuring process and the possibility of non-contact measuring techniques [3, 4, 5]. In contributing to the research of newly developed methods, it is important to understand the functionality of the heart, it's normality and abnormality, along with already used and new diagnostic techniques. This chapter will be devoted to deepen the understanding of this functionality and introduce used and new diagnostic techniques.

1.2 The Cardiovascular System

The cardiovascular system consists of the heart, the blood and the blood vessels. The heart is a hollow organ, located near the midline in the thoracic cavity of the body. It functions as a pump that pushes the blood through the blood vessels into two closed circulations (the systemic and pulmonary circulations), allowing an exchange of materials with the cells. The two circulations are arranged in series where deoxygenated blood from the systematic circulation is an input to the pulmonary circulation and oxygenated blood from the pulmonary circulation an input to the systematic circulation. [6, 7]

The heart consists of four chambers (left and right atria and ventricles) and four valves, as seen in figure 1.1. The four valves are controlled by pressure changes occurring as the heart contracts and relaxes. Each valve helps to ensure a one way flow of blood, by opening to allow blood to flow through and then closing to prevent backflow. [6, 7]

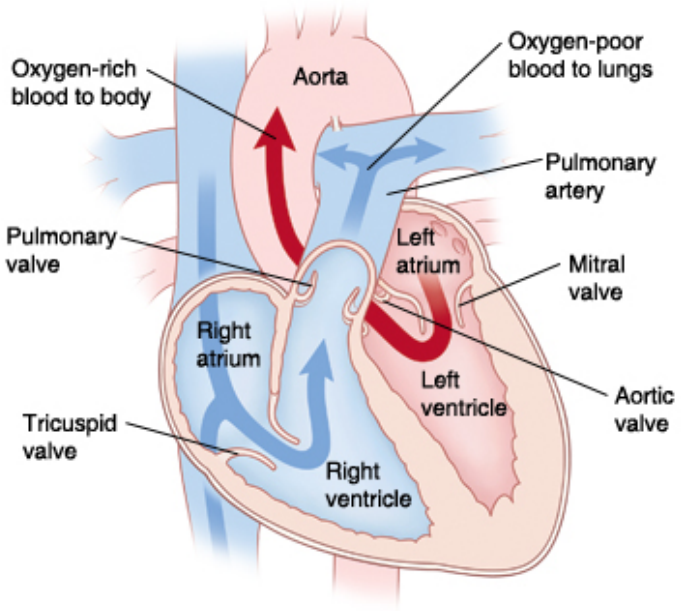

Figure 1.1: The heart consists of four chambers and four valves. The image shows how oxygenated (red) and deoxygenated (blue) blood travels through the heart. [8]

1.2.1 The Cardiac Cycle

The cardiac cycle consist of all of the electrical and mechanical events occurring during one heartbeat. Figure 1.2 shows a Wiggers diagram of the time variations in the electrical and mechanical events of the cardiac cycle. The chambers of the heart start with depolarization which leads to a contraction (systole) and relaxation (diastole) of the cardiac muscle fibers. This occurs simultaneously in the left and right side and asynchronous between the atria and ventricles, meaning that when the atria contract the ventricles relax. The cardiac cycle includes systole and diastole for all of the chambers but conventionally, it is described in terms of the left ventricle. Systole is defined as the period from the closing of the mitral valve until the closing of the aortic valve, or contraction of the left ventricle. This can be split into two phases, isovolumetric contraction and ventricular ejection. Diastole is defined as the rest of the cardiac cycle and can be split up into four phases; isovolumetric relaxation, early diastolic filling, diastasis and atrial contraction. [6, 9]

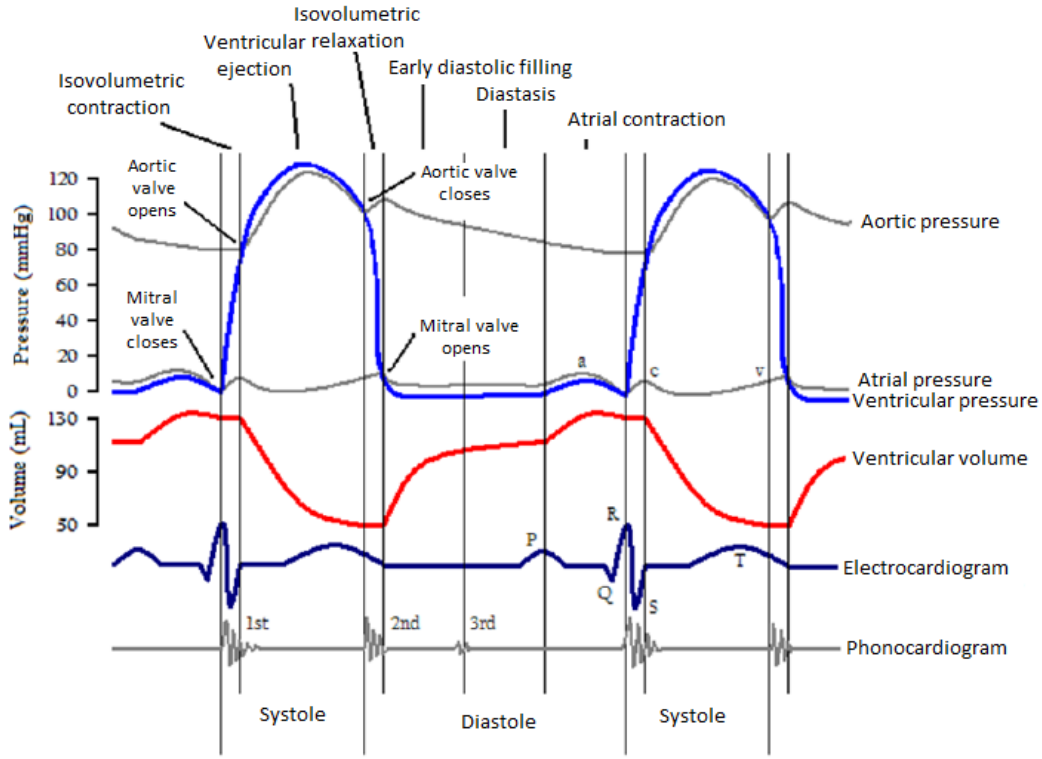

Figure 1.2: Wiggers diagram showing time variations in the electrical and mechanical events of the cardiac cycle. Modified from [10]

The mechanical cycle begins with **isovolumetric contraction** where all of the valves are closed and the left ventricle is contracting without changing in volume. Thus, the pressure inside the ventricle is increasing. As the pressure inside the left ventricle exceeds the pressure in the aorta, the aortic valve opens and **ventricular ejection** occurs. The blood flows through the valve causing the volume in the ventricle to decrease. Ventricular ejection terminates when the pressure in the aorta exceeds the pressure in the ventricle causing the aortic valve to close. At this point all of the valves are closed and an **isovolumetric relaxation** occurs where the pressure in the ventricles decreases. Isovolumetric relaxation terminates when the pressure in the left ventricle decreases below the left atrial pressure. This pressure change causes the mitral valve to open and **early diastolic filling** to occur where the blood flows rapidly into the ventricle. **Diastasis** occurs during the mid-portion of the diastole where the pressure in the left ventricle and the left atria equilibrates, causing the flow through the mitral valve to nearly stop. Following this, late in the diastole, the atria contracts (**atrial contraction**) causing the remaining 25% of the ventricular filling to occur. After the atrial systole, the atria relax causing the pressure to decrease below the pressure in the ventricle and the mitral valve to close, ending diastole. [6, 9]

1.2.2 The Atrioventricular and Semilunar Valves

There are two types of valves in the body, atrioventricular (AV) and semilunar (SL) valves. The AV valves (also known as the mitral and tricuspid valves) are thin, leaf like structures (cusps) that separate the atria and the connected ventricles. Figure 1.3 illustrates the mitral valve and its function. When the ventricles are relaxed, the cusps of the AV valves project into the ventricles and the blood flows from the atrium through the AV valves into the ventricles. When the ventricles start to contract, the pressure drives the cusps upwards toward

the atria. Eventually the edges reach each other and the valves close. The papillary muscles are connected to the cusps of the AV valves through the chordae tendineae and when the ventricles contract, the papillary muscles contract as well. This tightens the chordae tendineae which secures the closing of the valves and prevents the AV valves from opening upward and into the atria. [6, 7]

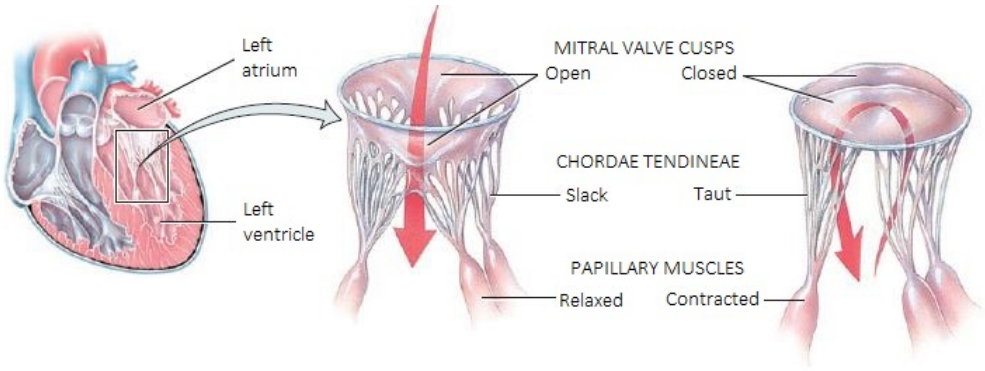

Figure 1.3: When the ventricles are relaxed, the chordae tendineae and papillary muscles are also relaxed causing the AV valve cusps to be open and blood to flow from the atria to the ventricles. When the ventricles start to contract, the papillary muscle contract causing the chordae tendineae to tighten and closing the cusps of the AV valve. Modified from [6]

The SL valves are made of pocket like structures, or three cusps. The aortic valve (left SL valve) separates the left ventricle from the aorta and the pulmonary valve (right SL valve) separates the right ventricle and the pulmonary artery. When the ventricles contract the pressure in the chamber builds up which eventually causes the SL valves to open, allowing blood to flow from the ventricles into the pulmonary trunk and the aorta. After contraction, the ventricles relax which causes the pressure to drop and the blood to flow back to the heart. This backflow fills the cusps of the SL valves which causes the edges to connect to each other and close the opening of the valves. If any of these valves is malfunctioning, a pathological condition occurs where the blood regurgitates or flows back to where it came from. [6, 7]

1.2.3 Heart Sounds

During each cardiac cycle, the mechanical operations of the heart produce vibrations that travel to the surface of the body and can be heard as sounds. The sounds are primarily caused by blood turbulence occurring during the closing of the heart valves but pathological sounds are often produced by narrowed or leaking valves. The sounds therefore provide information about the mechanical operation and can give an indication whether a pathological condition is occurring. [6]

Normal Heart Sounds

There are two fundamental heart sounds, S1 and S2 (see figure 1.4). S1 occurs soon after the ventricular systole begins and is caused by the closing of the AV valves. The sudden closing of the AV valves causes the blood to bounce back and hit the ventricular wall, causing it to

vibrate. This vibration then travels away from the valves and can be heard as a low frequency sound. It is often described as a "lub" sound. S2 occurs at the beginning of the diastole and is caused by the closing of the SL valves. As the SL valves close suddenly, the blood bounces back into the pulmonary artery and the aorta, making the walls of the arteries vibrate. These vibrations can be heard as a high frequency sound (relative to the low frequency S1 sound) and is often described as a "dub" sound, as it is lower and a bit shorter than S1. [6, 7]

Additionally, there are two extra heart sounds, S3 and S4, which can be heard in an abnormal heart (see figure 1.4). S3 occurs soon after S2 and is associated with blood turbulence during rapid ventricular filling in early diastole. S4 occurs just before S1 and is associated with blood turbulence during ventricular filling due to atrial contraction. [2, 6]

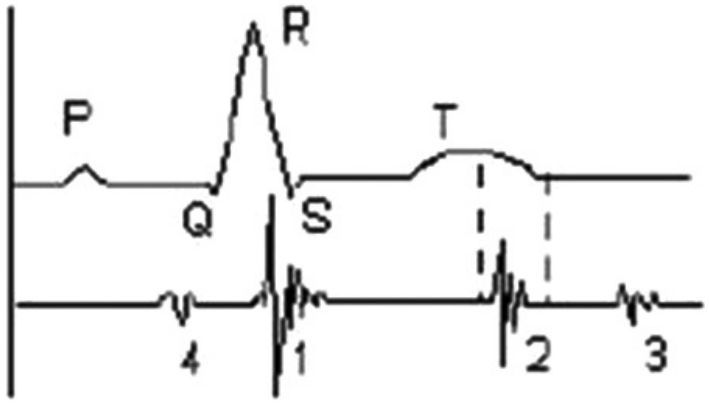

Figure 1.4: The heart sounds with ECG as a reference. S1 occurs as the AV valves shut and S2 as the SL valves close. S3 is associated with blood turbulence during rapid ventricular filling and S4 is associated with blood turbulence due to atrial contraction. [11]

Murmurs

Heart murmurs are unusual sounds such as clicking, rushing or gurgling. They are very common in children and usually thought to be an innocent finding which disappears with age. However, murmurs in adults most often indicate a malfunction in the operation of the heart valves. There are two types of heart valve disorders, insufficient opening and insufficient closing. A narrowing of the opening of a heart valve which causes restricted blood flow is known as stenosis and failure of the valve to close completely which results in a backflow of blood through the leaky valve is known as regurgitation or incompetence. [6, 12]

Heart murmurs can be classified as systolic murmurs which occur during the ventricular systole (period between S1 and S2) or diastolic murmurs which occur during the ventricular diastole (period between S2 and S1). The classification as well as the site of auscultation (listening to sounds within the body) can help in distinguishing between stenosis and regurgitation, i.e. systolic murmurs can be aortic stenosis, pulmonaric stenosis, mitral regurgitation or tricuspid regurgitation and diastolic murmurs are aortic regurgitation, pulmonaric regurgitation, mitral stenosis, tricuspid stenosis. [6, 12]

1.3 Diagnostic Techniques

Abnormal heart sounds or murmurs are often the first sign of a pathological condition and as in most disease early detection is favorable in giving an easier, more efficient and economical treatment [2]. Various measurements can be extracted for diagnostic purposes using different tools and methods. Measurements including information about for example heart rate (HR) and heart rate variability (HRV) are widely used. [3]
Additionally, displacement of the chest wall can give information about the hearts activity. The chest surface mainly moves because of respiratory activity but there are also smaller vibrations occurring due to the cardiac activity. The movement of the chest wall caused by respiratory activity ranges from 4 - 12 mm [13] at a frequency around 0.2 - 0.34 Hz [14]. The movement of the chest wall due to cardiac activity ranges from 0.2 - 0.5mm [15] at a frequency around 1 - 1.34 Hz [14]. [16]

Multiple diagnostic tools and methods are available for observing these measurements such as a stethoscope, seismocardiography, echocardiography and more.

1.3.1 Auscultation

Auscultation is the act of listening to the heart sounds, and other sounds originating within the body. Different areas of the chest wall can allow the listener to detect different malfunctions in the heart. Traditional sites are well described and include the Aortic Valve site, Pulmonic Valve site, Erb's Point, Tricuspid Valve site and the Mitral Valve site (see figure 1.5).
The sites are situated in different intercostal spaces on the thorax, bringing the listener closer to the origin of the sound. Generally, the first two heart sounds can be heard at each of the sites but abnormalities are often better heard at one site compared to another. [17]

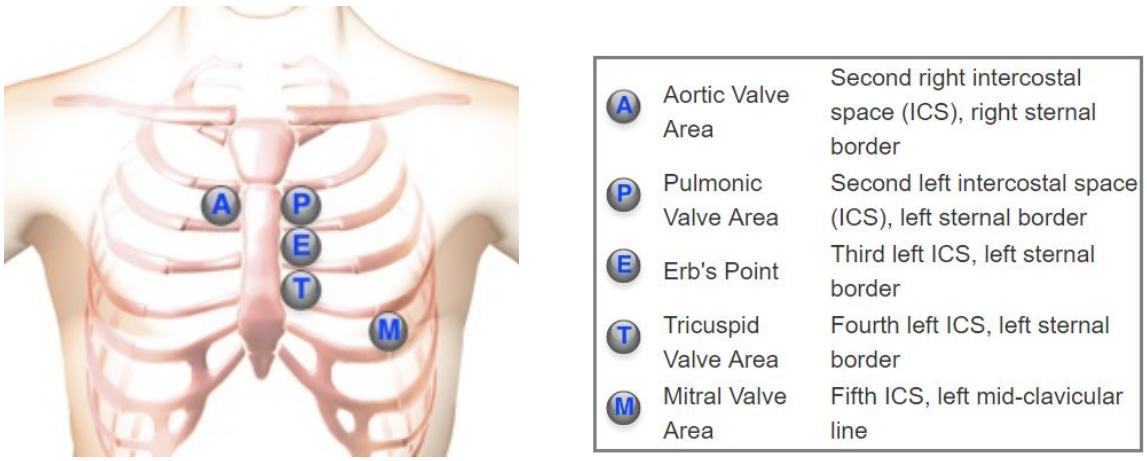

Figure 1.5: Traditional auscultation sites for listening to heart sounds. [18]

The Stethoscope

The stethoscope is the oldest tool used for auscultation. Before the stethoscope was invented the clinician listened to the heart by placing its ear on the thorax. In 1819, Laënnec published a thesis describing the first stethoscope which was a hollow cylinder made from light

wood that should be placed on the patients chest, transmitting sound to one ear. [17, 19] Since then, the design of the stethoscope has made great progress with additional features as well as more quality and comfort for the user. A stethoscope placed on a patients chest picks up vibrations at the thorax as pressure waves and directs them through a tube to the clinicians ears, where they are perceived as sound. These sounds usually have rather low amplitude and can be hard to hear. [17, 20]

The chest piece is the part of the stethoscope that touches the patient. It has two parts (usually on either side of the unit), the bell and the diaphragm (see figure 1.6). The bell is a hollow cup that transmits lower frequency sounds while the diaphragm is a disc that is able to transmit higher frequency sounds. In newer designs of the stethoscope, these two parts are in the same unit and the user controls the features by applying light pressure when using the bell and more pressure when using the diaphragm.
The tube carries the pressure wave from the chest piece to the listener's ears. Many variations exist, but in principle, with longer tubes more attenuation occurs as the sound travels from the chest piece to the ears.
The earpieces connect the stethoscope to the listener, allowing the pressure waves to travel directly into the listener's ears. [17, 20]

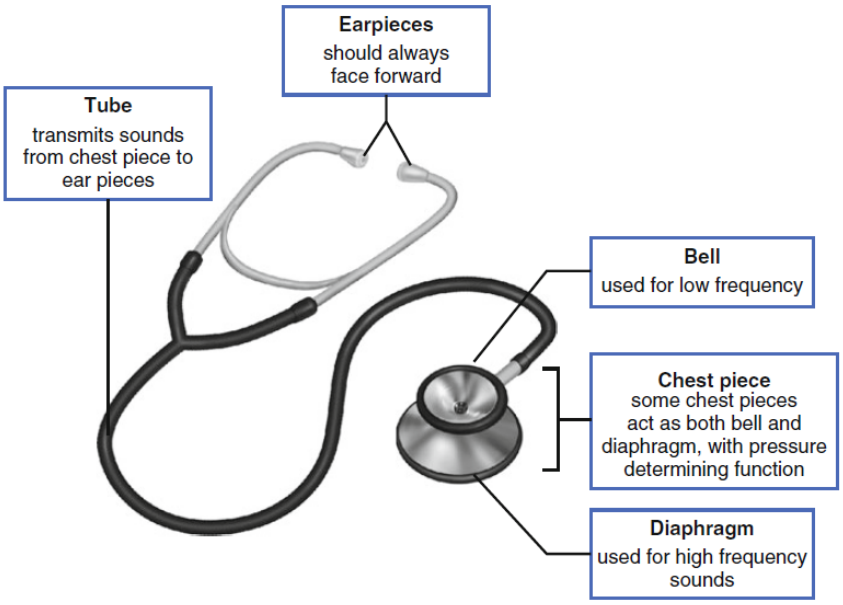

Figure 1.6: An example of an acoustic stethoscope [20]

Improved technology in the last few decades lead to the development of the electronic stethoscope in the early 2000s. Commonly, with the use of piezoelectric sensors, pressure waves are converted into analog electrical signals that can be A/D converted and processed by a computer. There are many advantages using the electronic stethoscope, e.g. amplification of sound output, frequency range enhancement, noise reduction and the possibility of recording and replaying via an external device. [21, 22]

1.3.2 Seismocardiography

Seismocardiography (SCG) is a method that utilizes the acceleration of the thorax wall and translates the changes to cardiac activity. The technique known today was first introduced in the early 1990s but came with bulky and expensive equipment [23]. Throughout the 1990s advances in imaging techniques such as echocardiography got more attention in the medical sector taking the focus away from SCG [24]. Great advances in technology, such as with micro electro mechanical systems (MEMS) in the last couple of decades has inspired researchers to revisit the method since MEMS allows for cheaper and lighter equipment with higher sensitivity. [25].
An accelerometer, usually consisting of piezoelectric sensors, is placed on the sternum in contact with skin. Vibration on the skin, originating from pressure waves generated by the hearts mechanism during each cardiac cycle, is measured in relevance to acceleration. An example of a typical SCG with an ECG as a reference is seen in figure 1.7. Since the acceleration is the second derivative to deformation it provides more information about the behavior of the signal. [25, 26, 27]

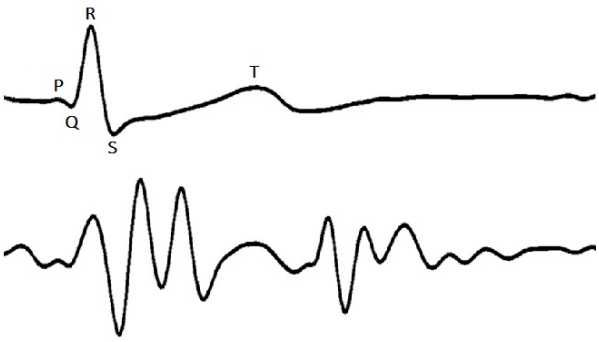

Figure 1.7: An example of an typical SCG signal in reference with an ECG signal. Modified from [26]

Seismocardiography is often measured by placing an accelerometer at the sternum using a double adhesive tape [24]. Applications include both low frequency measurements (below 25 Hz) as well as at higher frequency (up to 1 kHz), depending highly on the equipment, the sampling frequency and the purpose of the measurement [28].

Wave forms and their relation to physiological events of the low frequency SCG have been studied since mid 1900s. Mounsey [29] measured and related cardiac events to the wave deflection in the SCG. Others have related cardiac events to fiducial points on the SCG (e.g. Zanetti in 1991 [23] and Crow et al. in 1994 [30]). SCG is considered a reliable measurement and has been shown to produce stable results over time making it a useful method in measuring cardiac activity [23].

Although the diagnostic techniques mentioned in this section are reliable they have certain limitations. The main limitation is perhaps the requirement to be in contact with the device during the examination which can cause some inconvenience or irritation (e.g. patients allergic to the adhesive) and can even be inappropriate to some groups of patients (e.g. infants or burn victims). These limitations have raised the need for an alternative method

where contact is not needed and has led researchers throughout the world to examine other methods [4, 31, 32].

1.4 Alternative Techniques

Multiple non-contact methods have been examined as an alternative to the more conventional contact methods. Most of the newest and most promising methods for measuring HR and HRV are based on the vibrations on the surface of the body during the cardiac cycle. Periodic movements caused by the pumping of blood from the heart are reflected at the subjects surface and can give information, e.g. about the cardiac cycle frequency. These movements can be detected by utilizing sensors of adequate resolution which typically work on the principle of the Doppler effect and sense waves that reflect (echo) as a result of active transmission. [3, 4]

In 2014, Kranjec et al [4] performed a feasibility study where four promising non-contact techniques were examined at different distances from the surface of the body and compared to a reference ECG. The experiment was carried out simultaneously for all techniques, where the heart rate was measured using 6 different methods (lead I ECG (as a reference), CCECG, microwave radar, Ultrasound (US) radar, audio signal microphone and headphone audio contact method). The results showed that all of the methods were feasible. Furthermore, the signal to noise ratio (SNR) was calculated where the microwave radar showed the best results for distances below 10 cm and the US radar for distances above 10 cm.

The microwave and ultrasound measurement techniques are both based on the Doppler effect and the principle of radar; a device sensing continuous electromagnetic or sound waves. The frequencies and output power are directly linked to the sensitivity of the system where higher quantities result in more sensitivity to small displacements occuring on the chest wall. Although these two methods work on the same principle, there are differences. US emitting sensors send out high frequency sound waves which need a medium to propagate through while microwave emitting sensors are based on electromagnetic waves propagating at a higher speed than the US. [4, 5]

In 2017, Kranjec et al [5] followed up with his former study and performed a feasibility study with proof of concept of an assembled non-contact HRV measuring device. This was done in an laboratory setting with healthy subjects and in a clinical environment with pathological subjects. The measuring device was based on US radar where the jugular vein was measured. They demonstrated that this method has great potential but that further research and improvement is needed. Some of the factors that can be considered for improvement of their system were e.g. an inconvenient position of the patient, robustness of the system etc.

More studies have been conducted in investigating a similar method. Shirkovskiy et al [31] designed an ultrasonic diagnostic tool based on this method where 32 ultrasound transducers on 3 different panels were used to obtain a 3D seismocardiographic images of the thorax and abdomen. Jeger-Madiot et al [32] presented his method in 2017 where an ultrasound pulse wave was reflected off an elliptical acoustic mirror to get a focus point on the surface of the body. They also showed that this method works through clothing.

These studies have shown that it is feasible to detect cardiac activity with this technique. This could be a valuable tool in clinical settings along with out-of-hospital use, lowering the time and effort of cardiac activity recording. Furthermore, it could be of benefit in other

fields and applications, e.g. psycho-physiological studies of different groups of subjects (athletes, drivers or rehabilitation patients) [4].

The limitations these studies have in common is that the bandwidth of the system is very limited and that there is not very much known about the information present in the received displacement signal. Furthermore, the knowledge of how that information translates to physiological events is lacking. Apart from Shirkovskiy et al. [31], most of the studies use ECG or laser-doppler as a validation method but wavelet comparison with known methods has yet to happen. All of the previous studies commonly state that it needs more investigation on what potential and information it can contribute.

Chapter 2

Problem Statement

What information do different frequency bands of a contactless ultrasound cardio-vibrometer signal contain in terms of breathing, heart rate and valve sounds; and how does it compare with current seismocardiographic methods?

Based on this problem statement the following goals were set:

- Record contactless ultrasound cardio-vibrometer signals from different distances, with and without clothing.
- Obtain a baseband signal representing the displacement of the chest wall.
- Extract information from the displacement signal and interpret it with respect to physiological events in the cardiac cycle.
- Examine what effect different distances have on the signal's quality and what effect clothing has on the signal's quality.
- Examine how the obtained seismocardiographic waveform correlates with an accelerometer.

Part II

Problem Solution

Chapter 3

Methods

An experiment was performed to examine the information found in ultrasound vibrometer signals, which was encoded in a frequency modulated wave that had been reflected of a subject's surface. This chapter describes the method used in this project, starting with a theoretical background (section 3.1), followed by a description of the data acquisition procedure (section 3.2) and finally a description of the signal processing done in analyzing the signal (section 3.3).

3.1 Theoretical Background

This section describes the theory used in the experimental part of this project. First the theory behind modulating a signal is described, followed by an explanation of demodulation. Lastly, filters and filter design is explained.

3.1.1 Modulation

Modulation is a common method used in telecommunications and signal processing to transmit a baseband signal via a carrier wave with a fixed amplitude or frequency. There are many ways to modulate a signal but in principle an analog signal can be modulated in terms of its amplitude, frequency or phase. [33]

Amplitude modulation (AM) encodes the information in the carrier signal ($s_c = cos(\omega_c t)$) by modifying its amplitude, frequency modulation (FM) modifies its frequency and phase modulation (PM) modifies its phase. The difference between AM and FM can be seen in figure 3.1. FM and PM are highly related and are often referred to as angle modulation. [33]

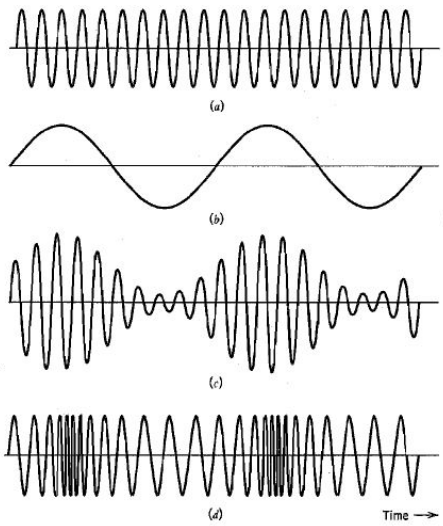

Figure 3.1: Difference between AM and FM. (a) The carrier wave, (b) the signal for modulation, (c) AM and (d) FM. [33]

As mentioned in section 1.4, when the heart pumps blood, periodic movements are reflected on the subject's surface. The displacement occurring on the surface can be measured using an ultrasound transmitter and receiver to measure frequency shifts related to the Doppler effect. Figure 3.2 shows how the transmitted signal is related to the reflected signal. As the wave gets reflected off the surface of the body, it gets frequency modulated. The modulated carrier signal ($s_m(t)$) can be represented in an equation as

$$s_m(t) = cos(\omega_c t + \phi(t))$$

where ω_c is the angular frequency of the carrier wave and $\phi(t)$ is the phase deviation from the carrier phase due to the movement of the chest wall. The time (Δt) it takes for the signal to travel from the emitter to the receiver is double the distance (d) to the reflecting surface divided by the traveling speed (c), $\Delta t = 2d/c$. The phase deviation ($\phi(t) = \omega_c \Delta t$) that occurs due to this time delay is thus

$$\phi(t) = \frac{2\omega_c}{c} x(t) \tag{3.1}$$

where $x(t)$ is the change in d over time (the displacement of the chest wall). This means that as the wavelength gets smaller, or as the transducer is operated at a higher frequency (as $\lambda = 2\pi c/\omega_c$), more sensitivity to smaller displacements is reached. [4]

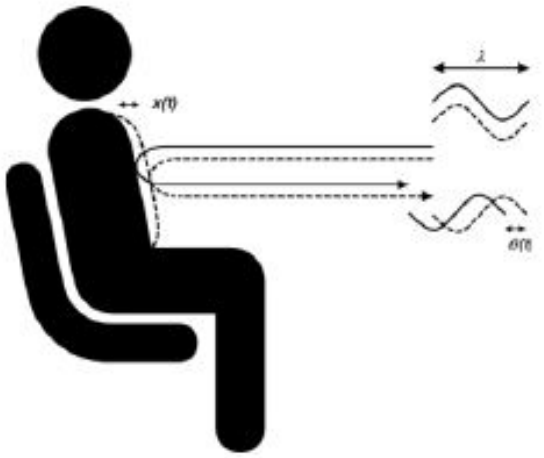

Figure 3.2: Doppler displacement where λ is the wavelength of the transmitted signal, $\phi(t)$ is the phase change due to $x(t)$ which is the displacement of the chest due to cardiac activity. [4]

3.1.2 Demodulation

After modulation and transmission, the transmitted signal is demodulated to extract the baseband signal. As with modulation, there are multiple ways to demodulate the signal. Quadrature demodulation is a method that is often used, where the FM signal is acquired by using quadrature signals generated from the modulated signal. One advantage of using this method is that quadrature demodulators can handle delay in the system that results in an unknown phase [34].

Quadrature Demodulation

A carrier signal which has been modulated, i.e. by reflecting off a subjects chest, represented by $s_m(t)$ can be written in the form

$$s_m(t) = A(t)cos(2\pi f_c t + \phi(t)) \tag{3.2}$$

where A(t) is the amplitude of the signal, f_c is the frequency of the carrier wave and $\phi(t)$ is the phase deviation from the instantaneous phase $2\pi f_c t$ (i.e. due to the movement of the chest wall). In an ideal case of an FM signal, $A(t)$ is a constant. The phase deviation, $\phi(t)$, can be written in relation to the deviation in frequency as $2\pi f_\Delta t$. [33, 35]

A complex envelope of the modulated signal can be generated and represented in a rectangular form as

$$\widetilde{s}_m(t) = I(t) + jQ(t) \tag{3.3}$$

The complex envelope, including the low pass in-phase (I) and quadrature (Q) components, contains all of the information found in the baseband signal. [33, 35]

In practise, I and Q components are obtained by multiplying $x_m(t)$ with sinusoids that have the same frequency as the carrier wave. As stated in equation 3.4, $s_I(t)$ (containing the I component and the carrier wave) is acquired by multiplying $x_m(t)$ with a sinusoid and, according to equation 3.5, $s_Q(t)$ (containing the Q component and the carrier wave) is acquired by multiplying $x_m(t)$ with a sinusoid which is phase shifted by 90 degrees from the previous sinusoid (cosine and sinus).

$$s_I(t) = x_m(t) * cos(2\pi f_c t) \tag{3.4}$$

$$s_Q(t) = x_m(t) * sin(2\pi f_c t) \tag{3.5}$$

The heterodyne principle states that two sinusoidal signals of two different frequencies which are mixed, can be written as the sum of two sinusoids where the frequencies are the sum and difference of the original frequencies [34]. It is based on the trigonometric identities:

$$cos(\theta_1)cos(\theta_2) = \frac{1}{2}cos(\theta_1 - \theta_2) + \frac{1}{2}cos(\theta_1 + \theta_2)$$

$$cos(\theta_1)sin(\theta_2) = \frac{1}{2}sin(\theta_1 + \theta_2) - \frac{1}{2}sin(\theta_1 - \theta_2)$$

Utilizing this, the following can be derived:

$$s_I(t) = \frac{1}{2}A(t)\Big(cos\Big(2\pi(2f_c + f_\Delta)t\Big) + cos\ \Big(2\pi f_\Delta t\Big)\Big) \tag{3.6}$$

$$s_Q(t) = \frac{1}{2}A(t)\Big(sin\Big(2\pi f_\Delta t\Big) + sin\ \Big(2\pi(2f_c + f_\Delta)t\Big)\Big) \tag{3.7}$$

It is assumed that the carrier frequency is much higher than the deviation frequency, and as seen from equations 3.6 and 3.7 the carrier wave can easily be filtered out using a low pass filter, leaving only the frequency component related to the displacement of the chest wall. [33, 35]

As the I and Q components can be written in a complex form (see equation 3.3) it can be illustrated in a phasor diagram as seen in figure 3.3. From the definition of complex numbers and as can be interpreted form the phasor diagram the instantaneous amplitude and phase

can be found using trigonometric identities. In FM, the signal can be demodulated by finding the instantaneous phase. The frequency can then be derived as the continuous phase change over time. It can be seen that the instantaneous phase, $\phi(t)$, is related to the I and Q components such that [33, 35]

$$\phi(t) = arctan\Big(\frac{Q}{I}\Big) \tag{3.8}$$

The displacement of the chest wall can be calculated by rearranging equation 3.1 and substituting ω_c with λ, such that

$$x(t) = \frac{\phi(t)\lambda}{4\pi} \tag{3.9}$$

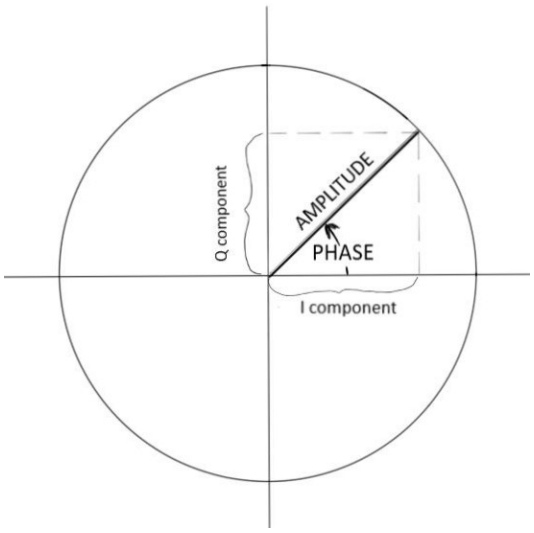

Figure 3.3: Phasor Diagram of I and Q components of the complex baseband signal

3.1.3 Filtering

The goal of filtering is essentially to reshape the spectrum of frequencies in order to get some advantage, for example in improving the signal to noise ratio (SNR). Usually bio-signals are narrow band, while noise is broadband. The filter can be designed in many ways, depending on what frequencies are of interest. It can be designed to pass low frequencies (Low-pass filter) where higher frequencies are attenuated, pass high frequencies (high-pass filter) where lower frequencies are attenuated or a mix of those two where frequencies of specific band are passed (Band-pass filter) and all other frequencies are attenuated. The gain of the filter is the ratio between the output voltage divided with the input voltage. When this ratio is given as a function of the frequencies, it is termed the transfer function. In designing a filter, the transfer function, representing the desired frequency response, needs to be defined. [35, 36]

Digital filtering

Digital filters can be based on analog prototypes (e.g. Butterworth, Chebyshev etc.) where an equivalent transfer function to the s domain transfer function of the analog filter is wanted. In determining the transfer function for the digital filter, the z-transform is very

useful because of its ability to define the digital equivalent of a transfer function. The digital transfer function is defined as

$$H(z) = \frac{Y(z)}{X(z)}$$

where Y(z) is the output and X(z) is the input. [35, 36]
The transfer function can be written in the form of a polynomials of z:

$$H(z) = \frac{b_0 + b_1 z^{-1} + b_2 z^{-2} + ... + b_N z^{-N}}{1 + a_1 z^{-1} + a_2 z^{-2} + ... + a_D z^{-D}}$$

From these two equations (assuming that $a_0 = 1$), the relationship between the output given any input can be determined as

$$\frac{Y(z)}{X(z)} = \frac{\sum_{k=0}^{N-1} b_k z^{-n}}{\sum_{l=0}^{D-1} a_l z^{-n}}$$

By multiplying and transforming this equation, the output in time domain can be written as

$$y[n] = \sum_{k=0}^{K} b_k x[n-k] - \sum_{l=1}^{L} a_l y[n-l]$$

The designing of an appropriate filter is simply determining the a and b coefficients such that the desired spectrum is acquired. The frequency response can be found by Fourier transforming the transfer function ($H(j\omega)$). [35, 36]
The order of the filter, or the complexity of the filter, is determined by the number of poles (coefficients in the denominator) in the transfer function. As the order of the filter increases the slope of the filters transition from pass-band to attenuation increases, approaching an ideal filter. However, approaching an ideal filter can cause a problem as the impulse response might become useless, causing a lot of ringing in the signal in time domain. A magnitude response of an ideal filter is seen in figure 3.4. The initial sharpness of the filter can be increased without increasing the order of the filter but by doing so, some unevenness or ripple will be present in the passband. In designing the filter, the order of the numerator (b-coefficients) must be equal or higher than the order of the denominator (a-coefficients) in order for the filter to be stable. [35, 36]

FIR and IIR

Filters can be separated into two groups according to their approach in reshaping the spectrum. These groups are finite impulse response (FIR) and infinite impulse response (IIR) filters. [35, 36]
The transfer function of FIR filters only include a numerator, meaning there are no a coefficients which operate on past values of the output. Thus, FIR filters only use the value of the input. The main advantage of FIR filers is that they are always stable (the order of the numerator is always higher than the order of the denominator) and have a linear phase shift. [35, 36]
The transfer function of IIR filters contain both a numerator and a denominator, meaning that the filter operates both on input values and past values of the output. [35, 36]
The advantage of choosing IIR filters over FIR filter, is that they usually require a much lower filter order in meeting a specific frequency criterion, and are more efficient in terms of computation time and memory. [35, 36]

In each group of filters (FIR and IIR), there are multiple designs. IIR filters are usually based on analog prototypes (e.g. Butterworth, Chebyshev etc.) although several computer aided designs have been developed. On the other hand, FIR filters are usually developed without an analog prototype. [35, 36]

Butterworth

The Butterworth filter design has often been used to smooth biomedical data (e.g. EMG signals, ECG signals, acceleration signals and more). It is known for its relatively flat pass- and stop-bands and its simple transfer function (Low-pass representation)

$$H(j\omega) = \frac{1}{\left(1 + \left(\frac{j\omega}{j\omega_c}\right)^2\right)^n} \tag{3.10}$$

where ω_c is the cut-off frequency and n is the filters order. Furthermore, the Butterworth filter design has shown good performance in reducing noise above the cut-off frequency. That is a very good property as biomedical displacement signals are often double-differentiated to obtain the acceleration, and as differentiation amplifies noise in the signal at high frequencies. [37]
The cut-off frequency is defined as the frequency point when the magnitude response of the filter has decreased 3dB from the pass-band magnitude. Compared to other IIR filters such as the Chebyshev (with a steeper transition between pass and stop-band and a controlled ripple in either the stop- or passband), the Butterworth design has very flat magnitude response in pass- and stop-bands, although the pass-stop band transition is relatively slower, see figure 3.4. Furthermore, the Butterworth has a relatively linear phase characteristic compared to the Chebyshev. [37]

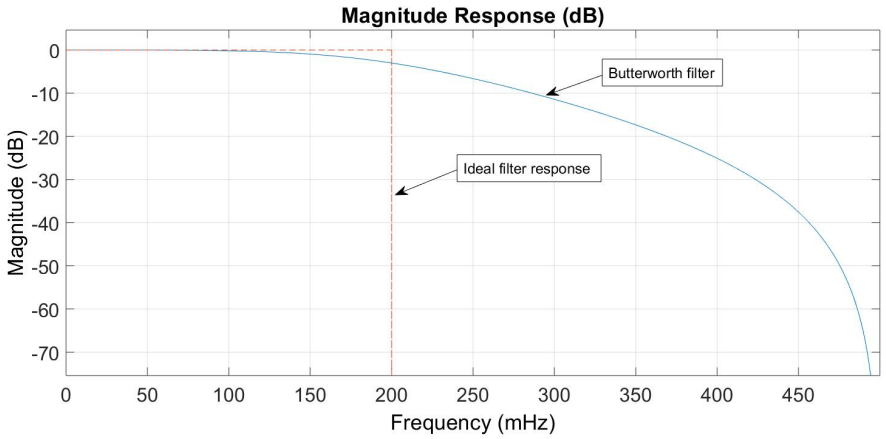

Figure 3.4: Example of a 2nd order butterworth filter, with cut-of frequency at 200 mHz and an ideal filter for comparison.

3.2 Data Acquisition

An experiment was performed where an ultrasound vibrometer signal was acquired from 13 healthy subjects. This section describes the equipment setup and the acquisition protocol.

3.2.1 Equipment Setup

A 40kHz continous ultrasound (US) wave was generated using an oscilloscope with wave form generator (Keysight EDUX1002G) and transmitted via an air-coupled ultrasound ceramic transducer (ProWave 400EP250). The transducer was located next to a condencer microphone (Avisoft Bioacoustics CM16/CMPA) that was placed directly in front of a subject (see figure 3.5). The reflected wave was then picked up by the microphone. The data was digitally sampled at 1MHz using a single channel recording system (UltraSoundGate 116H) and converted to a wav file using the supplied Avisoft-RECORDER software.

Simultaneously, a signal was recorded with an accelerometer (Silicon designs model 1521) placed on the lowest end of the sternum (xiphoid process). The acceleration data was digitally sampled at 5000 Hz using a data recorder (iWorx IX-214). This was used for comparison of waveforms between the accelerometer and the ultrasound. Both the ultrasound signal and accelerometer signals were processed in MATLAB.

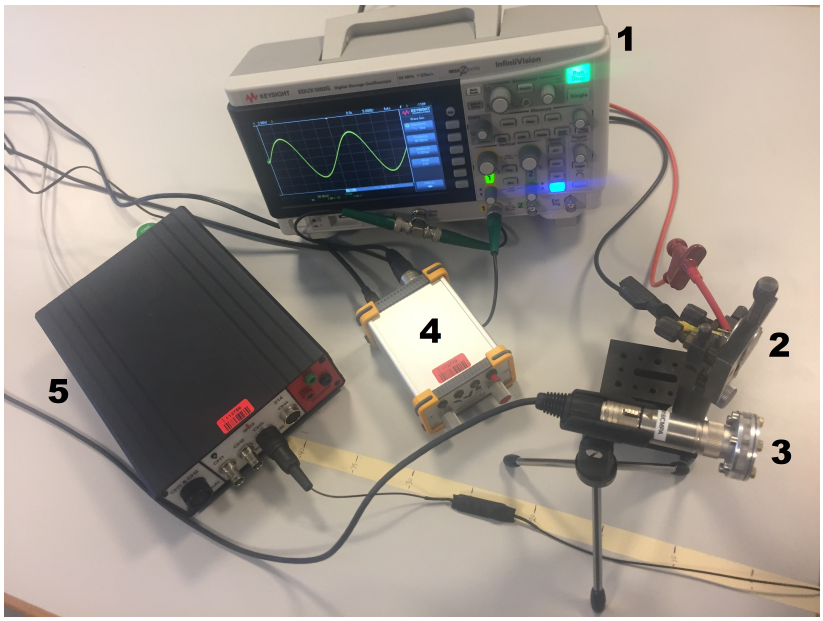

Figure 3.5: Setup of equipment for experiment. The oscilloscope (1) generated a 40kHz continuous US wave, which was transmitted via a US transducer (2). The condenser microphone (3) picked up the FM signal and sent it to a computer through the single channel recording system (4). Simultaneously, an accelerometer signal was recorded and digitally sampled using the data recorder (5).

3.2.2 Acquisition Protocol

Data was acquired from 13 healthy subjects although one reported having right bundle branch block (RBBB). Each subject was sat in front of the ultrasound transducer/microphone and was told to relax and breathe normally. The height of the chair was modified for each subject so that the microphone and transducer were aligned approximately to the fourth intercostal space (see figure 3.6). Two sets of measurements were recorded under two different conditions. One where the subject wore a cotton T-shirt and another where the subject sat without any clothing on (referred to as T-shirt ON/OFF later). Both sets had four measurements, taken from distances 10, 20, 30 and 40 centimeters. The sets and

measurements were taken in random order to avoid bias in data.

Figure 3.6: Subject sitting in front of the US transducer and microphone.

3.3 Signal Processing and Analysis

The acquired data was processed with a signal processing algorithm that was developed in MATLAB. The block diagram in figure 3.7 describes the process. The first step in processing the signal was to band-pass filter the data, followed by a baseband extraction. The baseband was extracted using the method in section 3.1.2 where a complex baseband signal was generated followed by a low-pass filter and arctan demodulation. The data was further processed using downsampling and high-pass filtering. Following this the signals were analyzed in terms of information in specific frequency bands using continuous wavelet transformation (CWT) and different filtering. Furthermore, the waveforms of the signals were compared to an accelerometer waveform. Lastly, fiducial points related to physiological events were transposed from acceleration to displacement US signal.

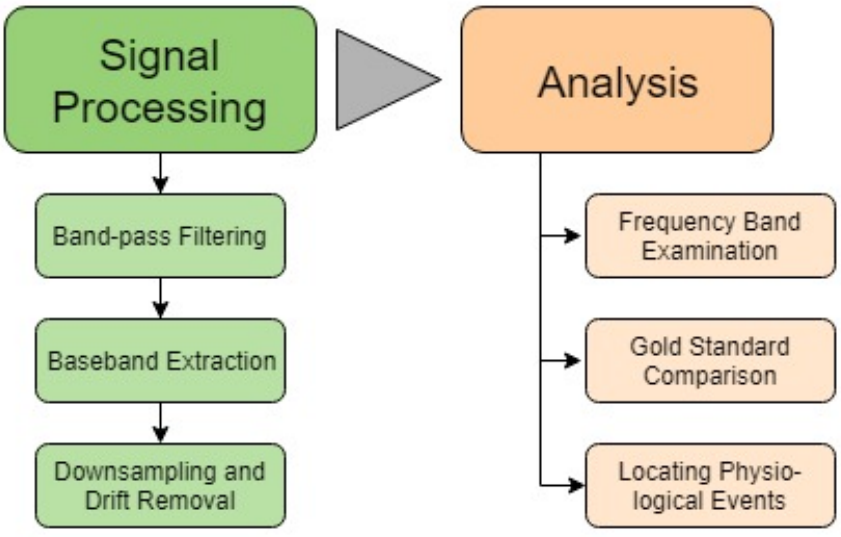

Figure 3.7: Block Diagram showing the steps taken in processing and analyzing the recorded signals.

3.3.1 Signal Processing

Band-pass filtering

The first step in processing the modulated signal was to filter it with a band-pass filter. This was done to eliminate the effect of harmonics. As mentioned in section 3.1.3, the desired frequency response needs to be specified when designing a filter. This means that the order (n) and the -3dB cutoff frequencies (ω) needed to be specified. A 4th order Butterworth band-pass filter was designed with cut-off frequencies at 37kHz and 43kHz. Second-order-sections (SOS) were generated from the filter coefficients and used to forward-backward filter (filter in both forward and reverse directions) the signal, thus doubling the filter order. Using SOS ensures that the filter is stable as the filter is then composed of multiple second order filters (and a first order filter if needed) [38].

Baseband Extraction

After implementing a band-pass filter, the dominant frequency in the signal was found and defined as the carrier frequency. This was done for different segments of the signal (first half, second half, middle part[1] and the full signal). The carrier frequency varied between segments and recordings. The most common frequency deviation was 0.2 Hz (see appendix A). The baseband was extracted in each segment of all of the signals according to the method in section 3.1.2 where first the complex baseband signal was generated, followed by low-pass filtering and arctan demodulation.

The complex baseband signal (the I and Q components) was generated as illustrated in figure 3.8 where first the band-pass filtered signal was multiplied with sinusoids, one 90° phase shifted in relation to the other (cosine and sinus). This led us to equations 3.6 and 3.7.

$$s_I(t) = \frac{1}{2}A(t)\Big(cos\Big(2\pi(2f_c + f_\Delta)t\Big) + cos\ \Big(2\pi f_\Delta t\Big)\Big) \qquad \text{(3.6 revisited)}$$

$$s_Q(t) = \frac{1}{2}A(t)\Big(sin\Big(2\pi f_\Delta t\Big) + sin\ \Big(2\pi(2f_c + f_\Delta)t\Big)\Big) \qquad \text{(3.7 revisited)}$$

As seen in these equations the carrier frequency f_c can be filtered out using a low-pass filter (f_c is considerably higher than the baseband frequencies f_Δ). Thus, a Butterworth low-pass filter was designed with a cut-off frequency at 1200 Hz and order 5. The signal was double-filtered using SOS.

[1] 20 second interval from second 10 - 30

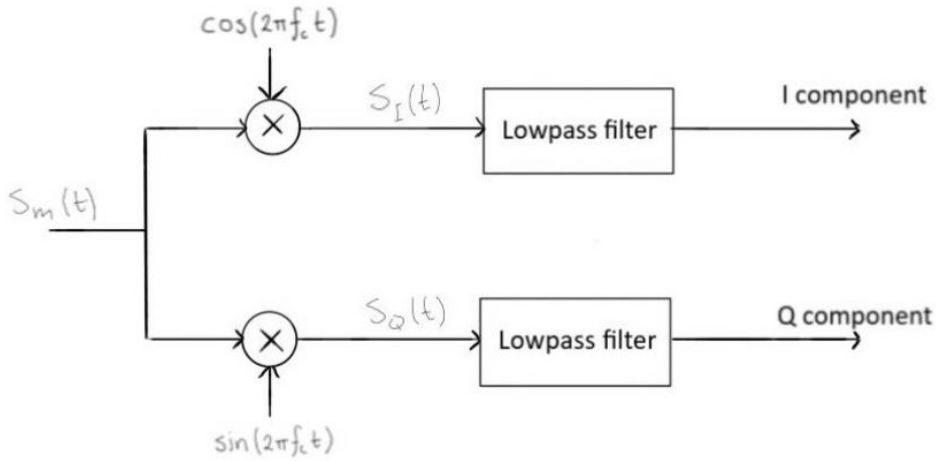

Figure 3.8: Block Diagram for generation of I/Q signals. The band-passed signal was multiplied with two sinusoids which were 90° phase shifted in relation to each other followed by low-pass filtering to obtain the I and Q components.

After generating the I and Q components, the phase deviation from the instantaneous phase $2\pi f_c t$ is found using an arctan demodulator. As mentioned in section 3.1.2, simple trigonometry allows us to calculate the phase deviation using

$$\phi(t) = arctan\Big(\frac{Q}{I}\Big) \tag{3.8 revisited}$$

The phase deviation, $\phi(t)$, is related to the displacement, $x(t)$, on the surface of the subject's chest, and is scaled by the wavelength of the transmitted signal, λ. The displacement can be written in an equation, and is given in meters by

$$x(t) = \frac{\phi(t)\lambda}{4\pi} \tag{3.11}$$

After demodulating all segments in all signals, a visual inspection was performed to select the segment with the best outcome. This segment was then used in further processing and analysis. In cases where the full signal had the best result, 20 seconds were selected from the signal.

Downsampling & Drift removal

The signal was oversampled at 1MHz, which then gave room for downsampling. In later stages the signal was differentiated in order to compare it with the accelerometer signal as a gold standard. When the sampling frequency was very high, the difference between two adjacent samples was very small which resulted in very small changes with differentiation. Therefore, by increasing the difference between two adjacent samples or downsampling, the representation of the derivative became better. Furthermore, the designing of a very low high-pass filter improved when the samples were reduced. Therefore, the signal was downsampled to 5kHz which was considered sufficient as the I/Q components had been filtered with less than half of that (1200 Hz).

After phase extraction and downsampling, the data contained a drift which was eliminated using a very low high pass filter. A Butterworth high-pass filter was designed with a cut-off frequency at 0.1 Hz and order 3. The signal was double-filtered using SOS.

3.3.2 Frequency Band Examination

For analysis of the signal, continuous wavelet transformation (CWT) was visualized on a magnitude scaleogram. Various high- and low-pass filters (see table 3.1) were designed based on energy distribution and/or interesting frequency bands in the signal. The filters where then used to either extracted these areas from the signal for analysis or to filter them out of the signal that was then analyzed further. All filters were Butterworth design and applied with forward-backward filtering using SOS.

Filter Name	**Filter Type**	**W_n [Hz]**	**Filter Order**
LP0.5	Low-pass	0.5	3
LP1.5	Low-pass	1.5	5
LP25	Low-pass	25	4
LP86	Low-pass	86	7
LPsub	Low-pass	subject dependant	4
HP0.1	High-pass	0.1	5
HP0.5	High-pass	0.5	3
HP0.6	High-pass	0.6	5
HP3	High-pass	3	5
HP25	High-pass	25	4

Table 3.1: Filters used for frequency band examination. All filters were Butterworth design and applied forward-backward, doubling the order presented here.

Information found in four different frequency bands (0.1-0.5 Hz, 0.6-3 Hz, 3-25 Hz and 25-86 Hz) of the signals were investigated in terms of amplitude. Average peak to peak amplitude in each signal was calculated by locating peaks in the signal associated to cardiac activity and finding their mean. The average peak to peak amplitude was then analyzed using a linear mixed model with distance and T-shirt ON/OFF as fixed factors. A subject specific random intercept was included in the model. P values < 0.05 were considered significant. In case of an interaction, multiple comparisons with Bonferroni corrections were performed. This was done separately for each frequency band. Analysis of the studentized residuals of raw data showed that assumption for normal distribution was violated (Shapiro-Wilk test, $p < 0.05$). Therefore, log transformation was applied to obtain normal distribution. Data is reported as mean $\pm$ standard error. Three signals were excluded from the statistical comparison as their mean peak to peak amplitude was largely influenced by demodulation errors and thus not representing the true amplitude of the baseband signal.

In assessing the noise floor in the signal, fourier analysis was performed on the raw signal, for all distances as well as T-shirt ON/OFF.

3.3.3 Gold Standard Comparison

For the purpose of comparing the ultrasound vibrometer signal with the accelerometer, the signal was double differentiated. Both the ultrasound vibrometer and accelerometer signals were filtered using a low-pass and a high-pass filter to secure same frequency band-width between the signals. Filters *HP3* and *LP25* were used. Both of the signals were forward-backward filtered using SOS.
The US vibrometer and accelerometer signals were taken simultaneously although some delay was introduced to the signals because of the software used and human variability. In order to compare the waves of the signals, one heart beat was manually selected in each vibrometer signal (for each distance and T-shirt ON/OFF) and the corresponding heart complex from the accelerometer signal. Thereafter, the two waveforms were cross-correlated to examine the similarities.

3.3.4 Locating Physiological Events

Physiological events related to the opening and closing of the heart valves were transposed form the acceleration US signal to the displacement US signal. The events included atrioventricular valve opening and closing and mitral valve opening and closing. The events were defined on the acceleration US signal according to a definition described by Sørensen et al. [39]. They were then transposed to the displacement signal according to the time points of the occurring events. The definition of the the events can be seen in figure 3.9.

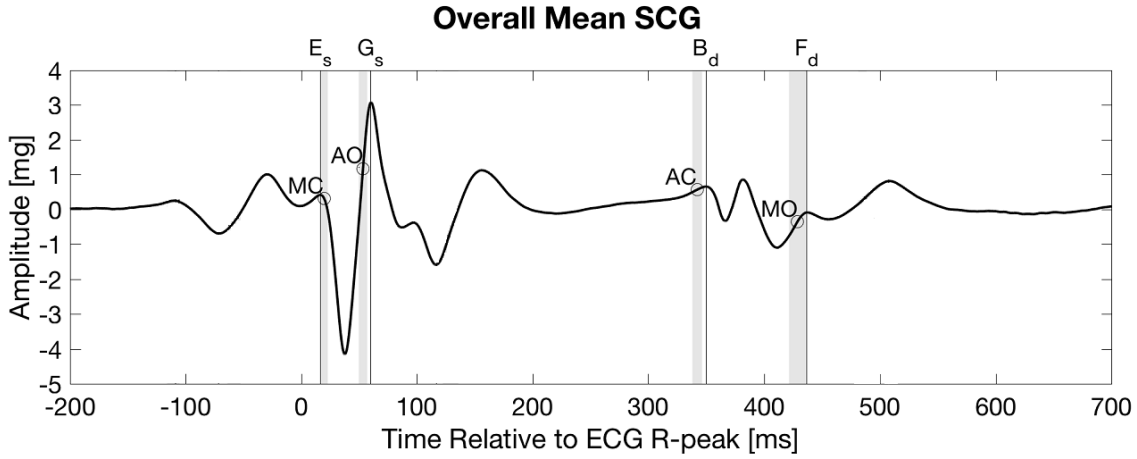

Figure 3.9: Four known physiological events located in an example seismocardiographic signal. The dots indicate the approximate location of the events (Mitral valve closure (MC), aortic valve opening (AO), aortic valve closure (AO), mitral valve opening (MO)). Modified from [39]

Chapter 4

Results

The following sections present the results from the frequency band examination and the result from the comparison of the US signal with the signal from an accelerometer as the gold standard.

4.1 Frequency Band Examination

The US signal's frequency spectrum was first analyzed as recorded (displacement), followed by analysis after transformation to velocity and acceleration.

4.1.1 Displacement signal

Figure 4.1 shows an example of a down-sampled US signal that had been filtered with *HP0.1* to remove drift.

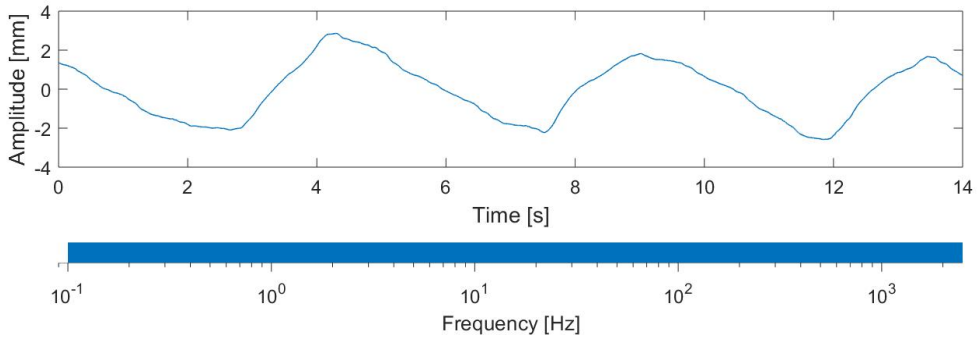

Figure 4.1: US frequency demodulated signal filtered at 0.1 Hz for drift removal. The signal shows displacement of an chest wall over time. The Frequency bar indicates the frequency bandwidth of the signal.

Figure 4.2 shows a magnitude scaleogram of the continuous wavelet transformation (CWT) of the signal. As seen, most of the frequency energy in the signal was constant over time at very low frequencies (less than 0.5 Hz).

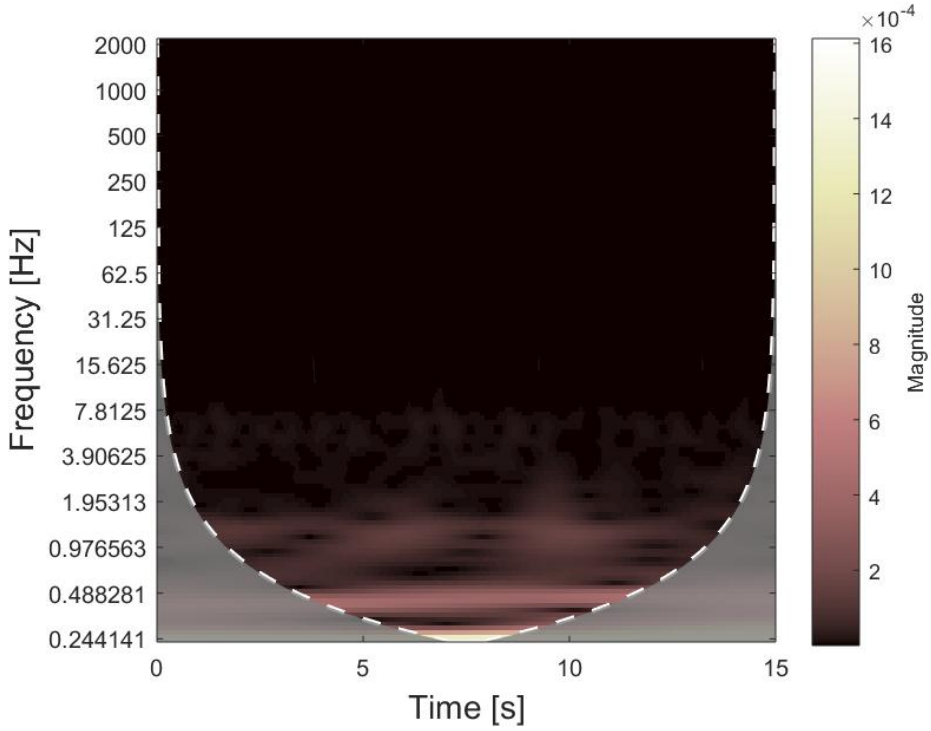

Figure 4.2: The magnitude scaleogram of an US signal, showing the energy of different frequencies. Most of the energy was present at very low frequencies (< 0.5Hz).

The US signal was filtered to take a better look at the information present in this frequency spectrum. Figure 4.3 shows the US signal after filtering, including frequencies above 0.1 Hz and below 0.5 Hz (*HP0.1* and *LP0.5*).

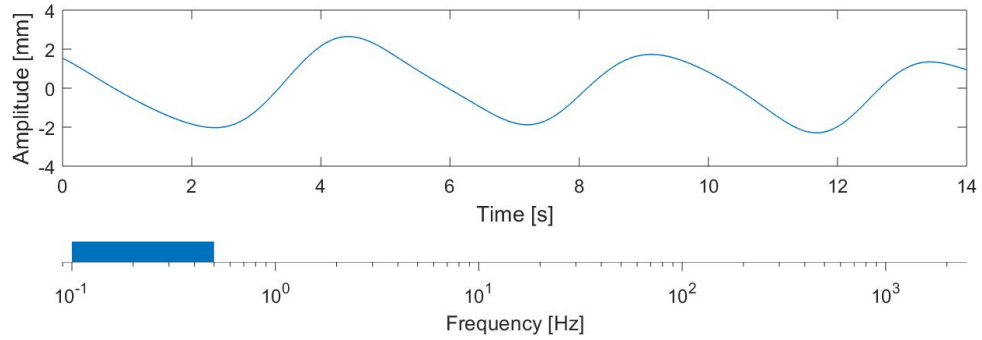

Figure 4.3: US signal filtered with filters *HP0.1* and *LP0.5*.

The average peak to peak amplitude and standard error for clothing and distance measurement of the US signals in this frequency spectrum is seen in figure 4.4. Interaction was found between clothing and distance, $F(3,81.16) = 6.957$, $p < 0.001$. This interaction is explained by a difference in amplitude between T-shirt ON/OFF only for measurements recorded at distance 40 cm ($p < 0.001$). Furthermore, a difference was found between measurements recorded at distance 40 cm, and distances 30 cm ($p = 0.006$), 20 cm ($p = 0.003$), 10 cm ($p = 0.001$), only for T-shirt ON. No differences were found for T-shirt OFF ($p > 0.05$, Bonferroni correction).

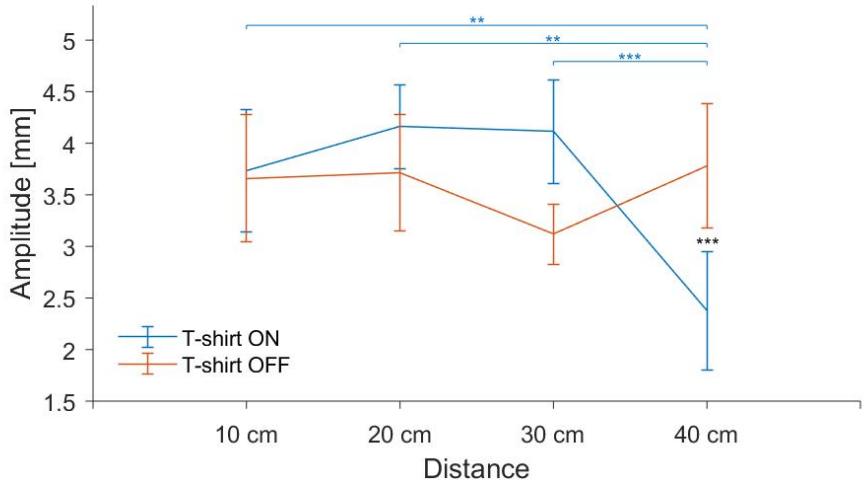

Figure 4.4: Mean peak to peak amplitude for each measurement of the US signal filtered with *HP0.1* and *LP0.5*. T-shirt ON is represented by blue and T-shirt OFF by red. Asterisks indicate significant differences found using post hoc comparison with Bonferroni correction. (** = $p \leq 0.01$, *** = $p \leq 0.001$)

Eliminating this frequency spectrum from the US signal with a high-pass filter allowed for further examination of information at higher frequencies. Figure 4.5 shows the signal after filtering with filter *HP0.5*.

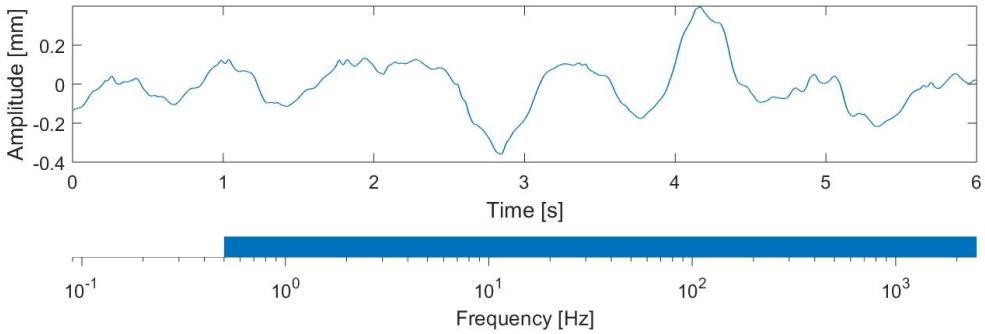

Figure 4.5: US signal over time filtered with *HP0.5*.

A magnitude scaleogram of the filtered US signal is shown in figure 4.6. The scaleogram shows that the magnitude of frequencies below 3 Hz is very similar over time but above approximately 3 Hz it becomes periodic.

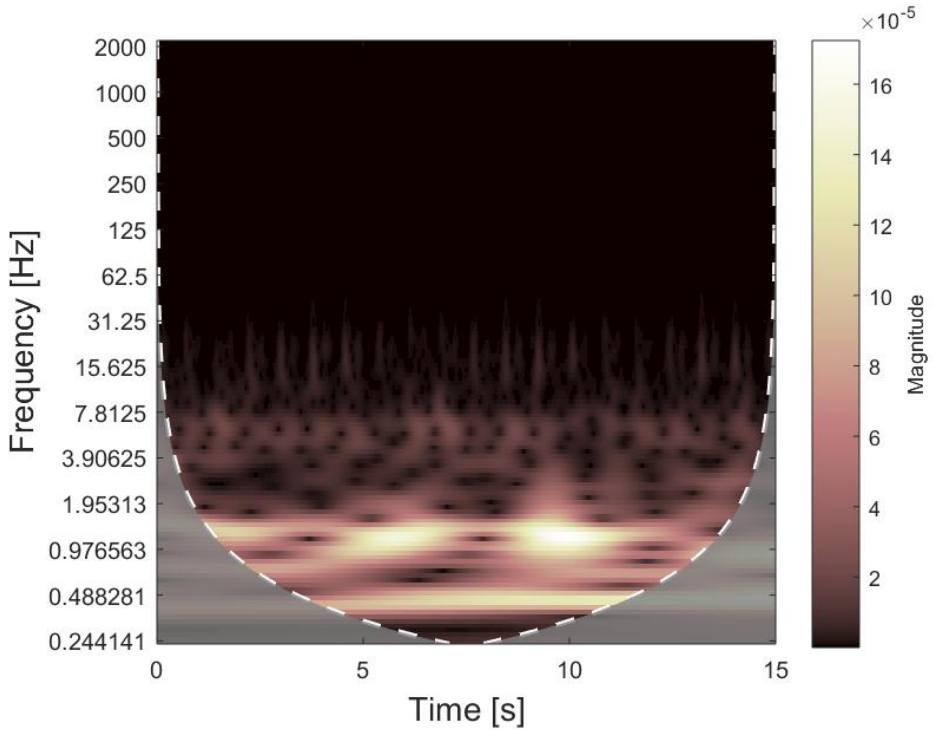

Figure 4.6: A magnitude scaleogram of the US signal filtered with filter *HP0.5*. Frequencies that are higher than 0.5Hz became more visible.

The US signal was filtered again to take a better look at the information present in the frequency spectrum above 0.5 Hz and below 3 Hz. Figure 4.7 shows the US signal after filtering with filters *LP0.6* and *HP3*.

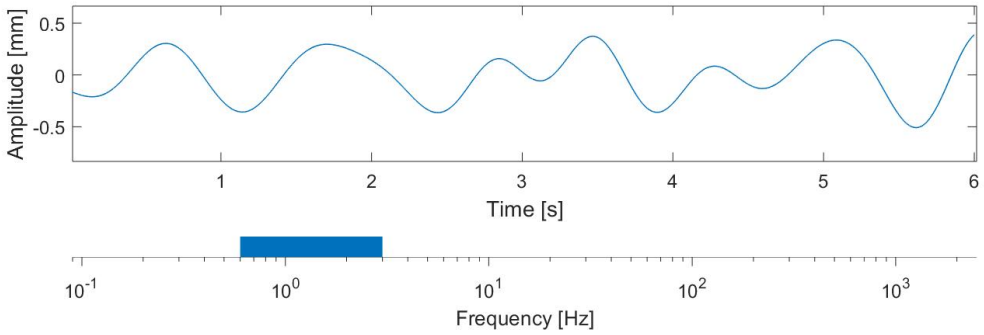

Figure 4.7: US signal filtered with filters *HP0.6* and *LP3*.

The average peak to peak amplitude and standard error for clothing and distance measurement of the US signals in this frequency spectrum can be seen in figure 4.8. No interaction was found between T-shirt ON/OFF and distance, $F(3,81.06) = 1.031$, $p = 0.383$. Furthermore, no main effects were found, neither for clothing ($F(1,81.07) = 0.03$, $p = 0.862$) nor for distance ($F(3,81.07) = 0.822$, $p = 0.485$). This indicates that the amplitude is the same regardless of clothing and the distance.

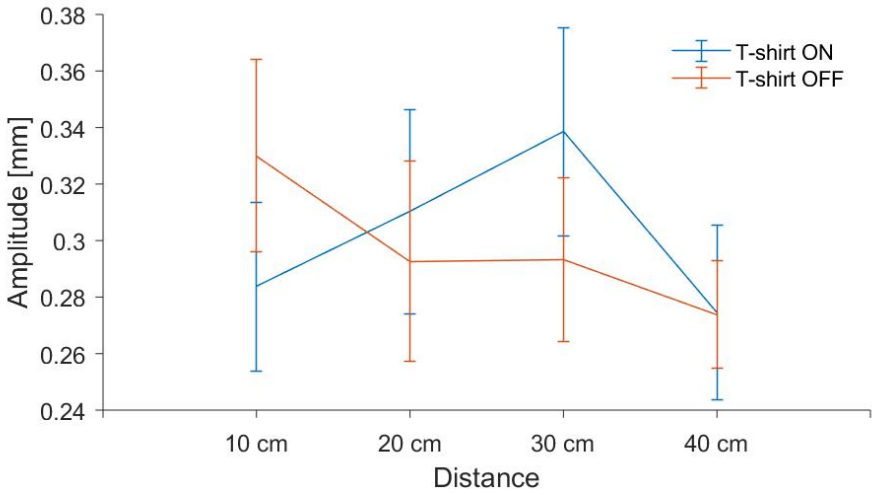

Figure 4.8: Mean peak to peak amplitude for each measurement of the US signal filtered with *HP3* and *LP0.6*. T-shirt ON is represented by blue and T-shirt OFF by red.

The frequency spectrum below 3 Hz was removed to allow for a further examination of higher frequencies. The magnitude scaleogram for the US signal above 3 Hz is seen in figure 4.9. The magnitude of frequencies above 3 Hz and up to approximately 25 Hz became more visible and are seen in a repetitive pattern.

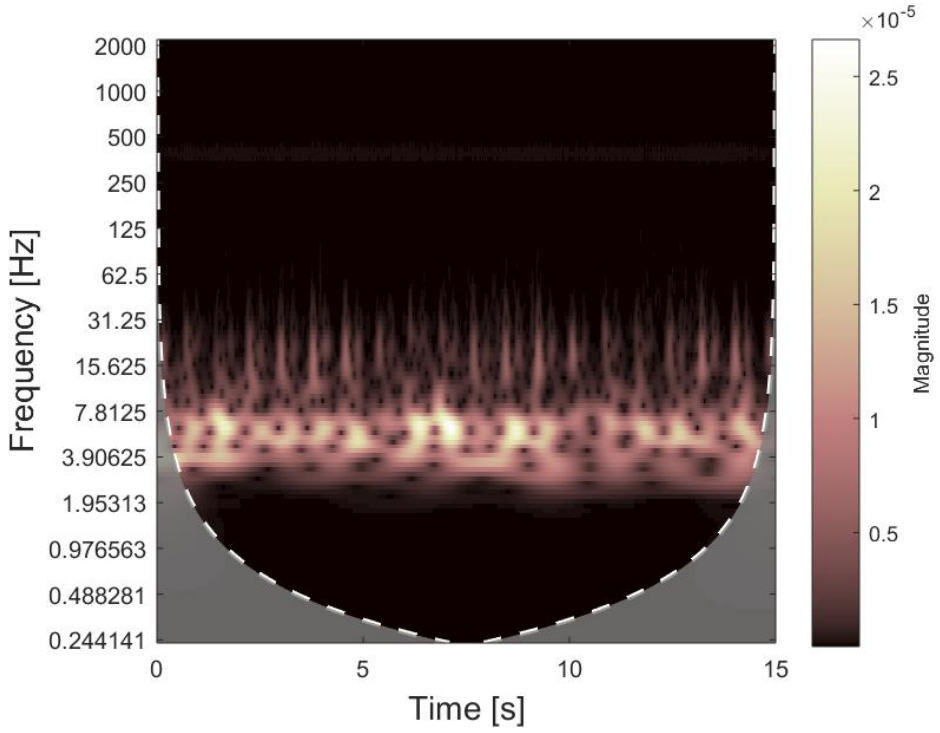

Figure 4.9: A magnitude scaleogram of the US signal filtered with high-pass filter *HP4*. The energy of the heart rhythm became more visible here, showing a repetitive pattern through time.

The US signal was filtered to examine the information present in the frequency band from 3 Hz to 25 Hz. Figure 4.10 shows the US signal filtered with filters *HP3* and *LP25*. Repetitive

pattern was present (pointed out with red arrows) where a "M" pattern occurs approximately every second.

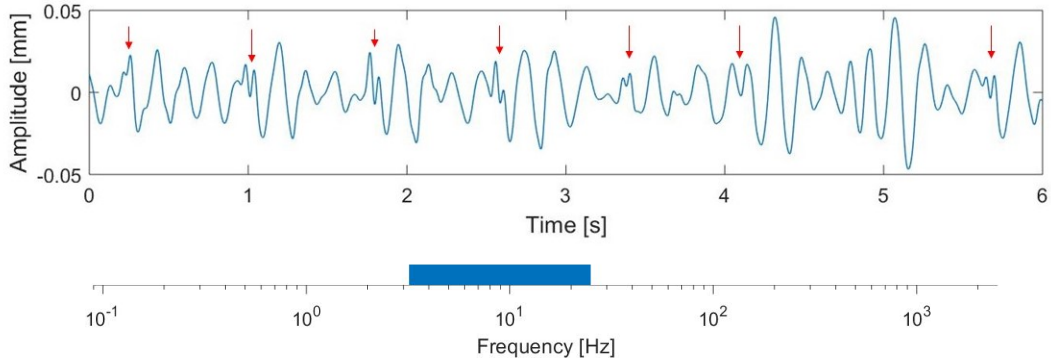

Figure 4.10: An US signal filtered with filters *HP3* and *LP25*. Red arrows point out repetitive "M" pattern in the signal. The derivative of this frequency part of the signal is used later in comparing with the golden standard and locating events in the cardiac cycle.

The average peak to peak amplitude and standard error for clothing and distance measurement of the US signal in this frequency spectrum can be seen in figure 4.11. Interaction was found between clothing and distance, $F(3,80.91) = 2.848$, $p = 0.043$. This interaction is explained by a difference in clothing only for measurements recorded at distance 30 cm ($p = 0.032$, Bonferroni correction).

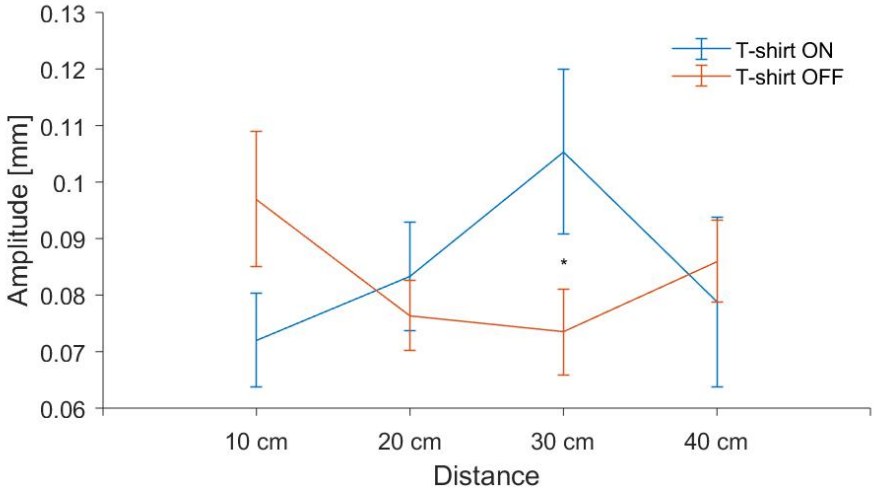

Figure 4.11: Mean peak to peak amplitude for each measurement of the US signal filtered with *HP25* and *LP3*. T-shirt ON is represented by blue and T-shirt OFF by red. Asterisks indicate significant differences found using post hoc comparison with Bonferroni correction. (* = $p \leq 0.05$)

The US signal was filtered with filter *HP25* to examine higher frequencies. Figure 4.12 shows the high-pass filtered US signal.

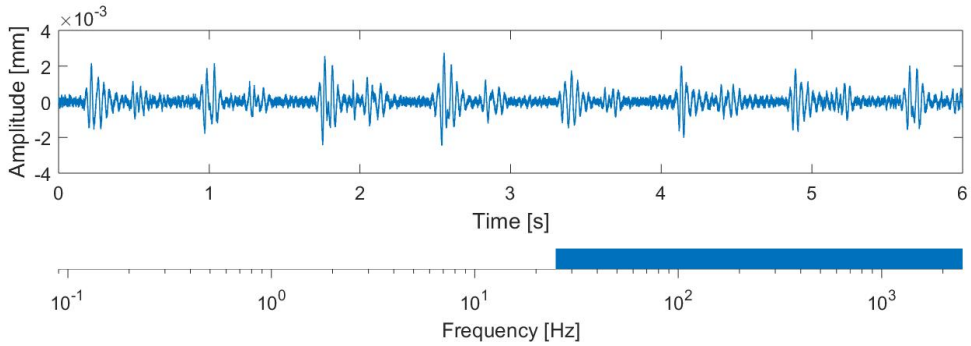

Figure 4.12: The US signal filtered with filter *HP25* reveling some heart sound pattern.

A magnitude scaleogram of the US signal including frequencies above 25 Hz is shown in figure 4.13. A band of high frequencies across the whole signal is clearly visible. This was found in all subjects, although it was located at different frequencies for each subject, ranging from approximately 190 - 630 Hz with a mean of 335 Hz.

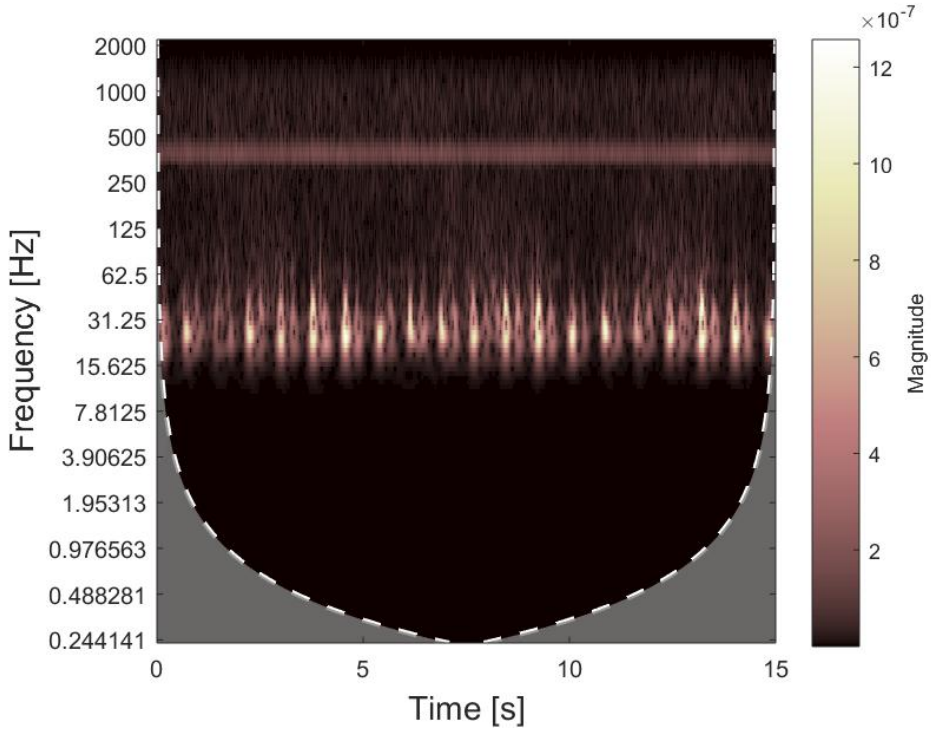

Figure 4.13: A magnitude scaleogram of the US signal filtered with filter *HP25*. The energy in the heart sounds became very visible here. The high frequency band was seen in all subjects.

Figure 4.14 shows the effect of low-pass filtering right below this frequency band which is at 325 Hz for this subject (red) (Filter *LPsub*). Furthermore, it shows the effect from low-pass filtering right above where most of the energy was found, around 86 Hz (yellow).

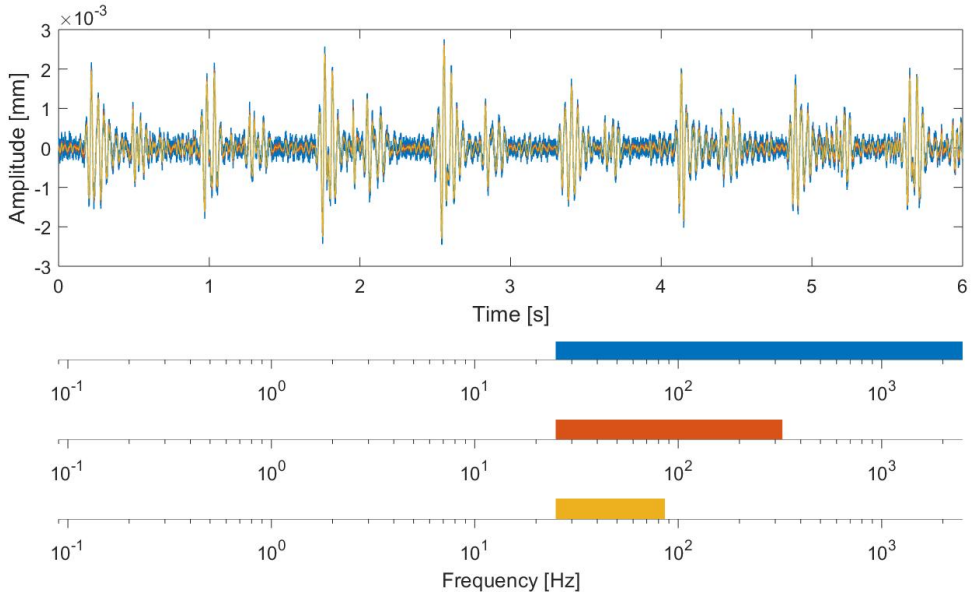

Figure 4.14: The US signal filtered with filter *HP25* is seen in blue. There is a lot of noise present although the heart sounds can be located. The red line shows the US signal filtered with *LPsub* at 325 Hz (specific for this subject). The noise level reduced slightly, making the heart sounds more visible. Lastly, the red line shows the US signal after low-pass filtering with filter *LP86*.

The average peak to peak amplitude and standard error for clothing and distance measurement of the US signal in the frequency spectrum of the signal filtered with *HP25* and *LP86* (yellow) can be seen in figure 4.15. Interaction was found between clothing and distance, $F(3,81.19) = 3.457$, $0 = 0.02$. This interaction is explained by a difference in clothing only for measurements recorded at distance 10 cm ($p = 0.021$, Bonferroni correction).

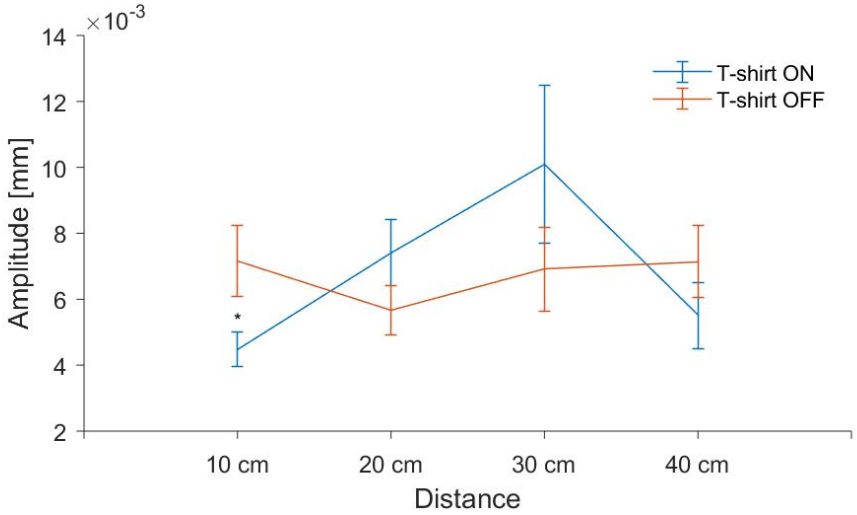

Figure 4.15: Mean peak to peak amplitude for each measurement of the US signal filtered with *HP86* and *LP25*. T-shirt ON is represented by blue and T-shirt OFF by red. Asterisks indicate significant differences found using post hoc comparison with Bonferroni correction. (* = $p \leq 0.05$)

Noise Floor and Distance Effect

An example showing the effect of distance on an US signal (T-shirt ON) which has been filtered with *HP25* and *LP86* is seen in figure 4.16. S1 and S2 can be seen at all distances although when examining all of the subjects the signal lacked quality at larger distances, meaning that noise was introduced at random times.

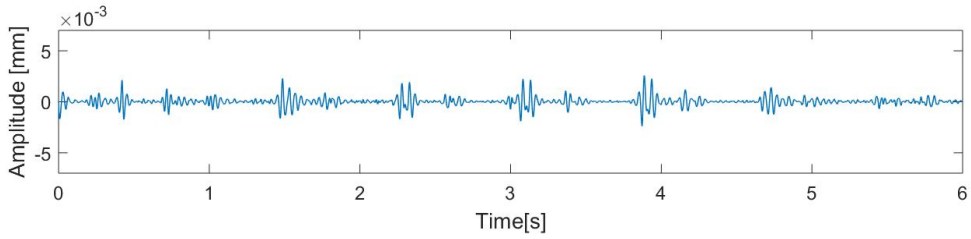

(a) T-shirt ON, distance 10 cm

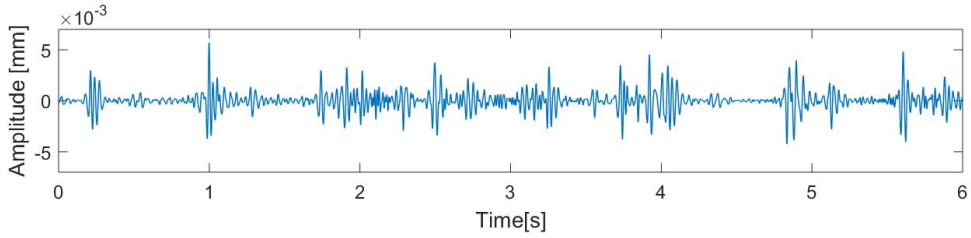

(b) T-shirt ON, distance 20 cm

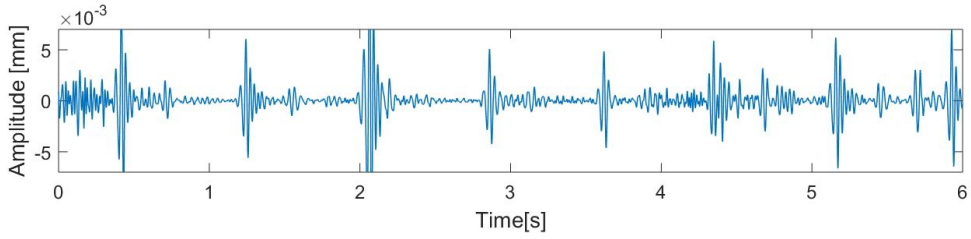

(c) T-shirt ON, distance 30 cm

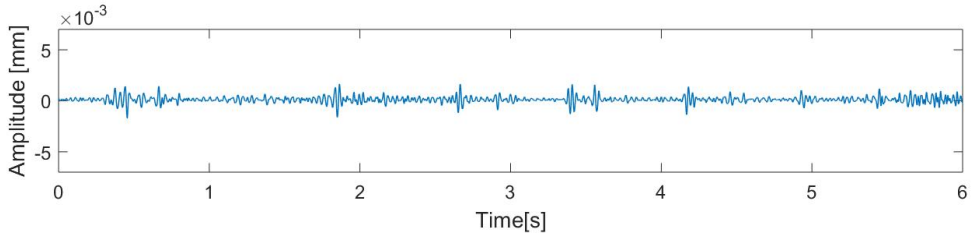

(d) T-shirt ON, distance 40 cm

Figure 4.16: The US signal (T-shirt ON) filtered with filters *HP25* and *LP86*. The effect of distance can be seen here. The quality of the signal is decreased at 40cm although heart sounds can be located at all distances.

Figure 4.17 shows another example of the effect of distance on an US signal (T-shirt OFF) which has been filtered with *HP25* and *LP86*. This signal has more constant quality over all distances compared to T-shirt ON in figure 4.16 .

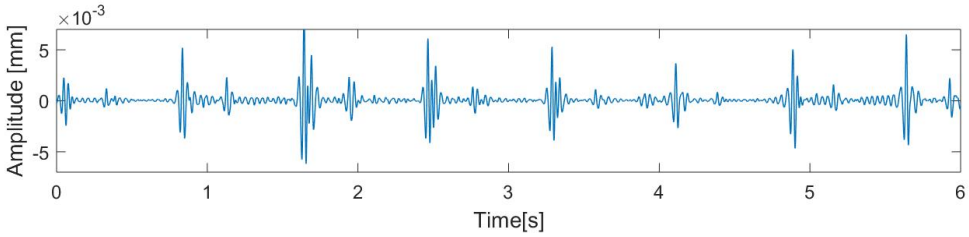

(a) T-shirt OFF, distance 10 cm

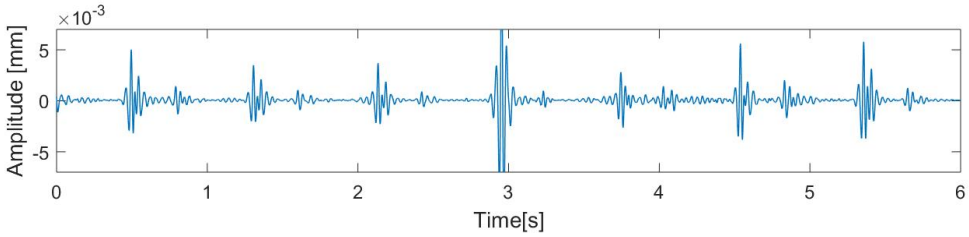

(b) T-shirt OFF, distance 20 cm

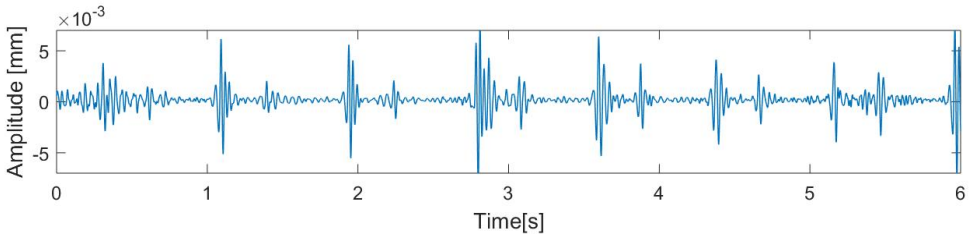

(c) T-shirt OFF, distance 30 cm

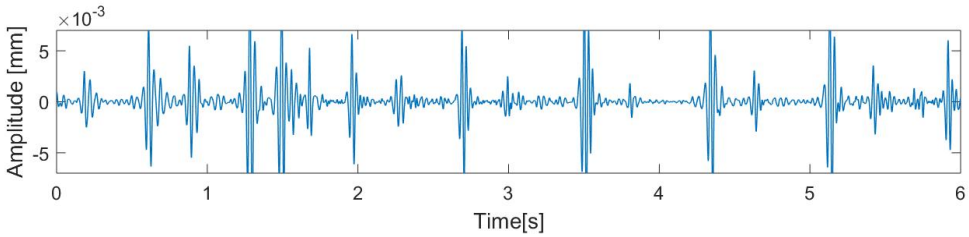

(d) T-shirt OFF, distance 40 cm

Figure 4.17: The US signal (T-shirt OFF) filtered with filters *HP25* and *LP86*. The effect of distance can be seen here. The quality of the signal is decreased at 40cm although heart sounds can be located at all distances.

Figure 4.18 shows a typical example of the amplitude spectrum of the unfiltered US signal (regardless of T-shirt ON/OFF and subject) in the frequency domain for all distances with T-shirt ON. Difference between subjects included e.g. amount of noise in the signal, as well as the location of the high frequency spike (pointed out with a red arrow in figure 4.18a). Low frequencies are dominant in the signal. The amplitude of each frequency is decreases with higher frequency. Almost all of the signals show little activity above 100Hz, apart from the spike mentioned earlier which is usually followed by increased noise. None of the signals had a definitive noise floor present.

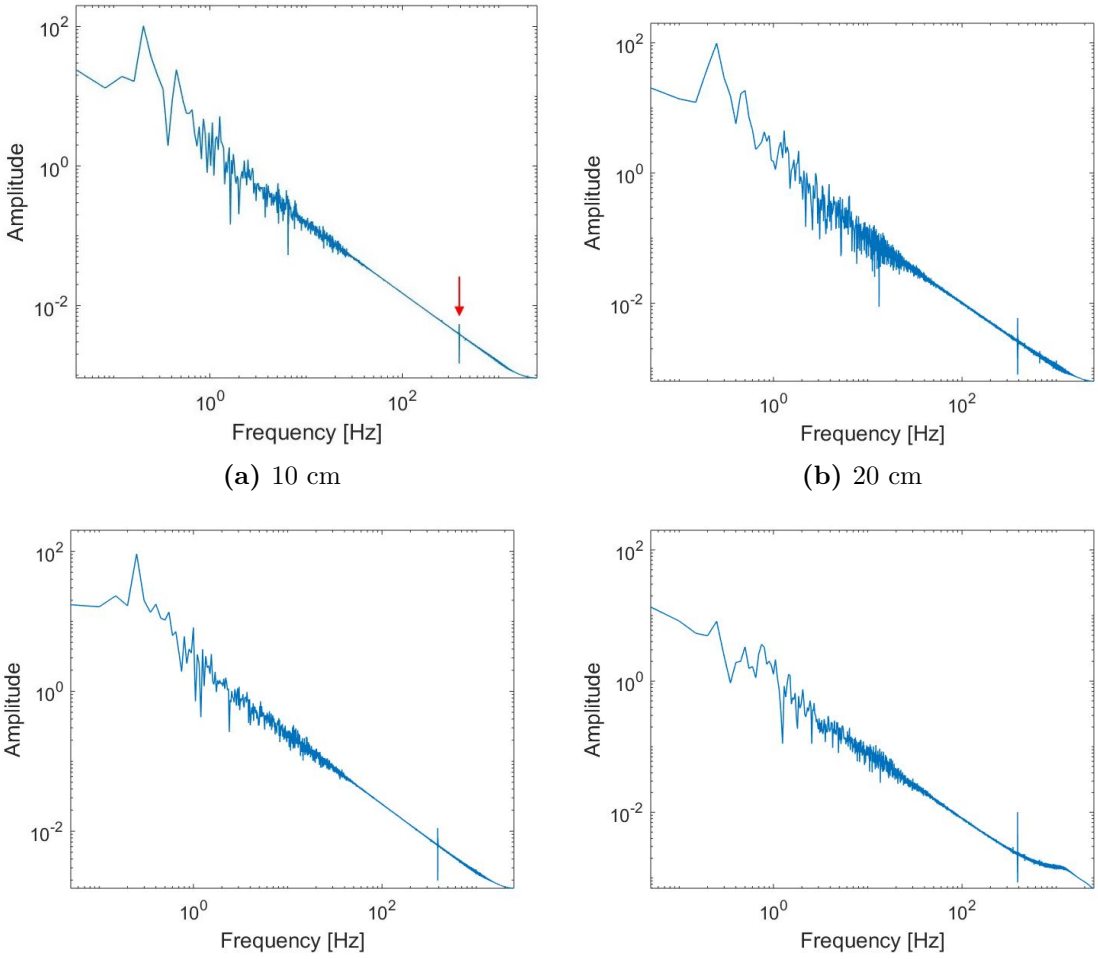

(a) 10 cm **(b)** 20 cm

(c) 30 cm **(d)** 40 cm

Figure 4.18: The amplitude spectrum of the unfiltered US signal in the frequency domain with T-shirt ON. Four different distances are shown, **(a)** 10 cm, **(b)** 20 cm, **(c)** 30 cm, **(d)** 40 cm. The red arrow in **(a)** points at a peak visible in the amplitude spectrum for all distances as well as T-shirt ON/OFF, although its location is subject dependent.

4.1.2 Velocity and Acceleration

An example US signal after transformation from displacement to velocity and acceleration is seen in figure 4.19. The displacement US signal has been differentiated (once to obtain velocity, twice for acceleration) and then filtered with *HP0.1*. Increased noise is introduced with each differentiation.

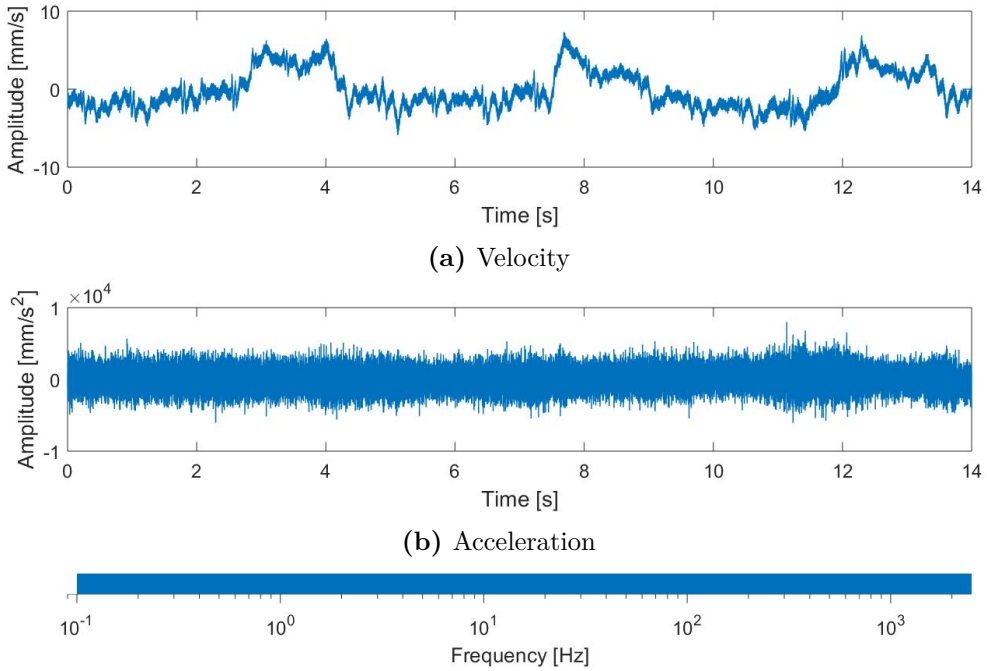

(a) Velocity

(b) Acceleration

Figure 4.19: US signal filtered using *HP0.1* and transformed into **(a)** velocity and **(b)** acceleration

The transformed US signals were analyzed using same filters as were used with displacement. Figure 4.20 shows an example US signal which was filtered with *HP3* and *LP25*. After filtering, heart rhythm could be seen clearly in the acceleration US signal.

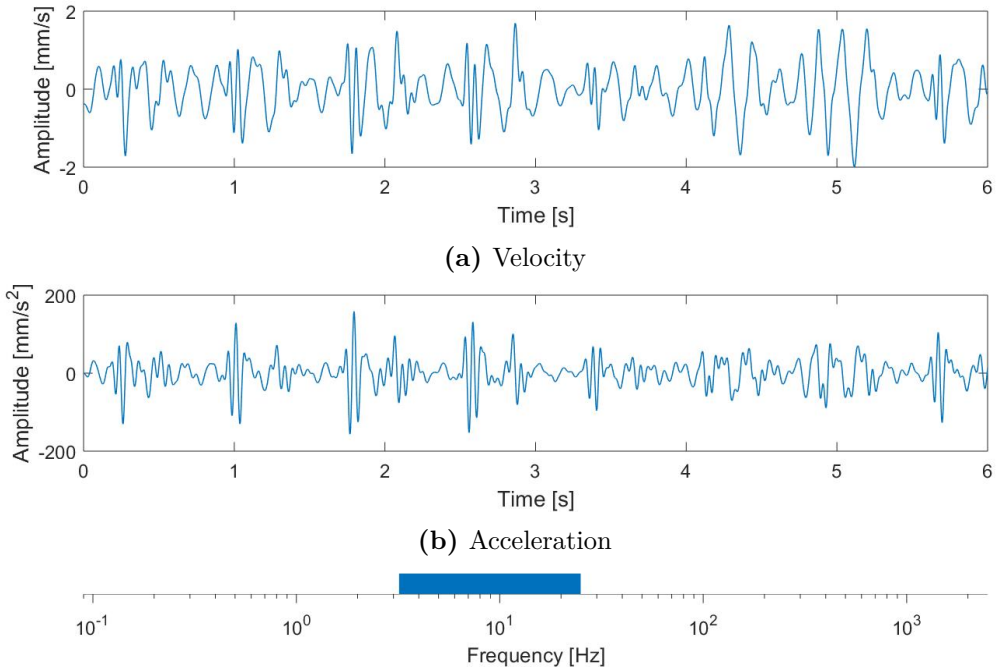

Figure 4.20: US signal transformed into **(a)** velocity and **(b)** acceleration and filtered using *HP3* and *LP25*.

Figures 4.21 and 4.22 show the average peak to peak amplitude and standard error for each condition and distance measurement of the velocity and acceleration signals which were filtered with *HP3* and *LP25*. Transforming the data from displacement to velocity and acceleration does not change the distribution of the data, thus the statistical results for the displacement was considered transferable to velocity and acceleration.

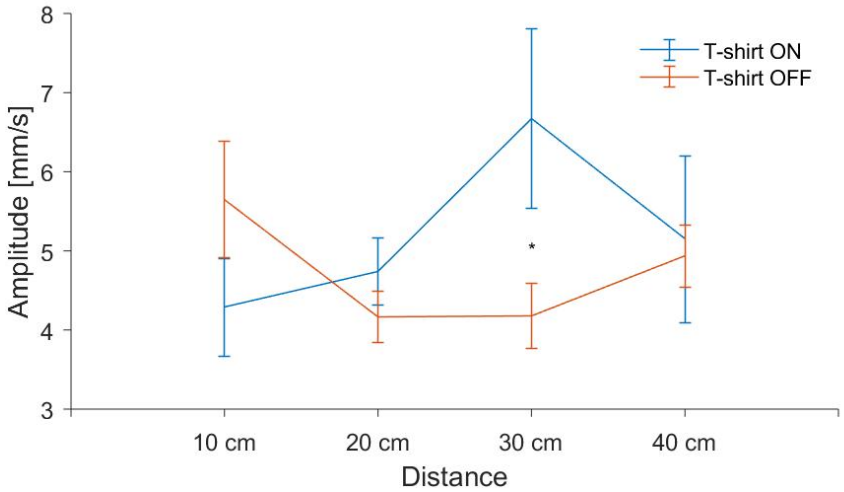

Figure 4.21: Mean peak to peak amplitude for each measurement of the differentiated US signal filtered with *HP25* and *LP3*. T-shirt ON is represented by blue and T-shirt OFF by red. Asterisks indicate significant differences found using post hoc comparison with Bonferroni correction. (* = $p \leq 0.05$)

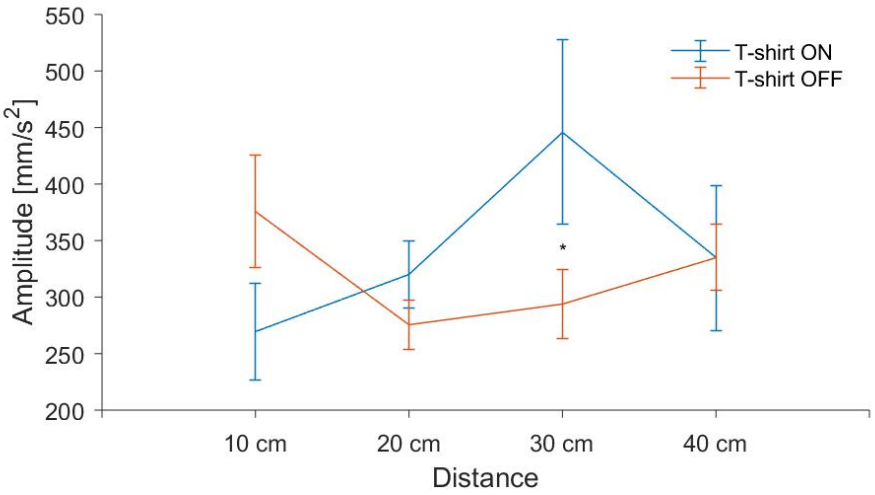

Figure 4.22: Mean peak to peak amplitude for each measurement of the differentiated US signal filtered with *HP25* and *LP3*. T-shirt ON is represented by blue and T-shirt OFF by red. Asterisks indicate significant differences found using post hoc comparison with Bonferroni correction. (* = $p \leq 0.05$)

Figure 4.23 shows three example velocity US signals, filtered at different frequencies. The blue is the velocity US signal which was high-pass filtered with *HP25*. The blue signal was then filtered with *LPsub* at around 325 Hz and with filter *LP86* (red and yellow, respectively). High frequency noise in the signal hid the heart rhythm information, although with selective filtering it was retrieved.

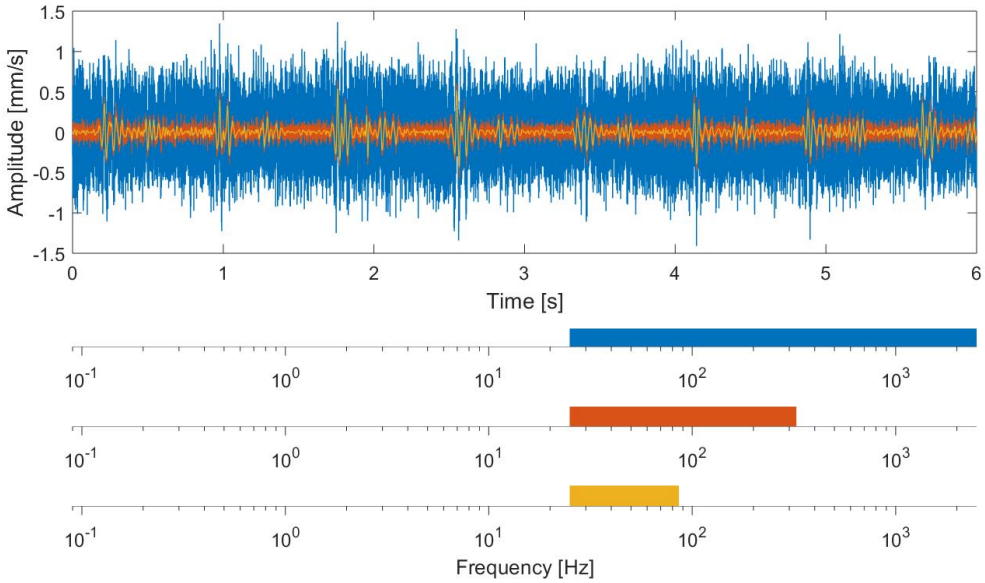

Figure 4.23: The velocity US signal filtered with filter *HP25* is seen in blue. That signal is then filtered with *LPsub* at 325 Hz (specific for this subject), shown in red. The noise level was reduced, making the heart sounds more visible. Lastly, the yellow line shows the signal when filtered with filter *LP86*.

Figure 4.24 shows two example acceleration US signals. The acceleration US signal was filtered using *HP25* as well as *LPsub* at 325 Hz and with filter *LP86* (red and yellow, respec-

tively). Unlike the displacement and velocity signals, high frequency noise was prominent in the signal and the hearth rhythm only got visible when low-pass filtering the signal at 86 Hz.

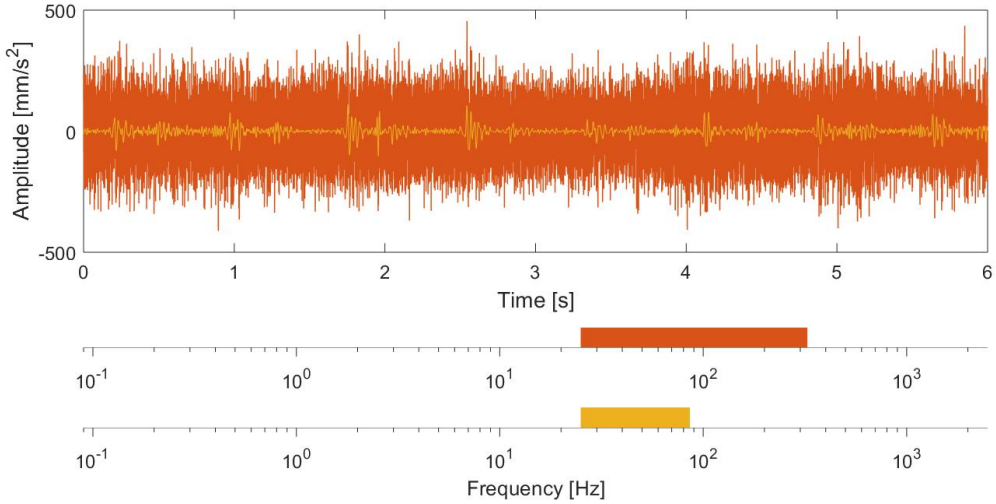

Figure 4.24: The acceleration US signal filtered with filters *HP25* and *LPsub* at 325 Hz (specific for this subject)is seen in red. The yellow line shows the US signal after filtering with filters *HP25* and *LP86*.

Figures 4.25 and 4.26 show the average peak to peak amplitude and standard error for each condition and distance measurement of the velocity and acceleration signals filtered with filters *HP25* and *LP86*. Transforming the data from displacement to velocity and acceleration does not change the distribution of the data, thus the statistical results for displacement was considered transferable to velocity and acceleration.

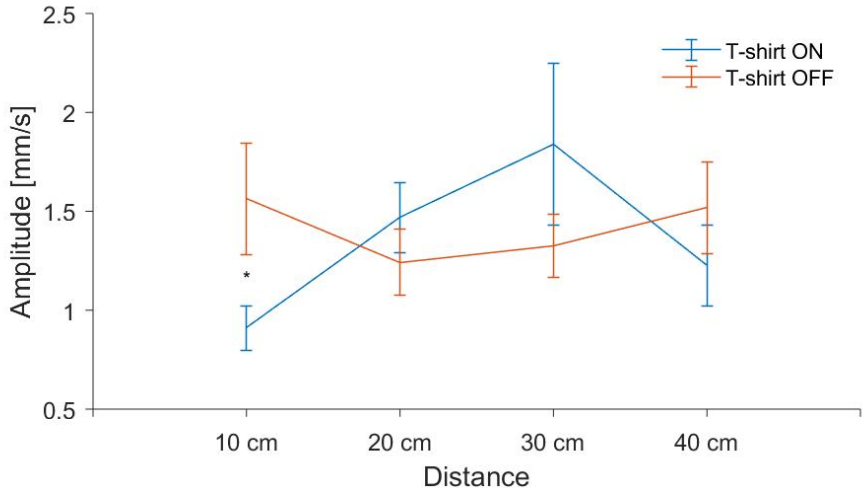

Figure 4.25: Mean peak to peak amplitude for each measurement of the differentiated US signal filtered with *HP86* and *LP25*. T-shirt ON is represented by blue and T-shirt OFF by red. Asterisks indicate significant differences found using post hoc comparison with Bonferroni correction. (* = $p \leq 0.05$).

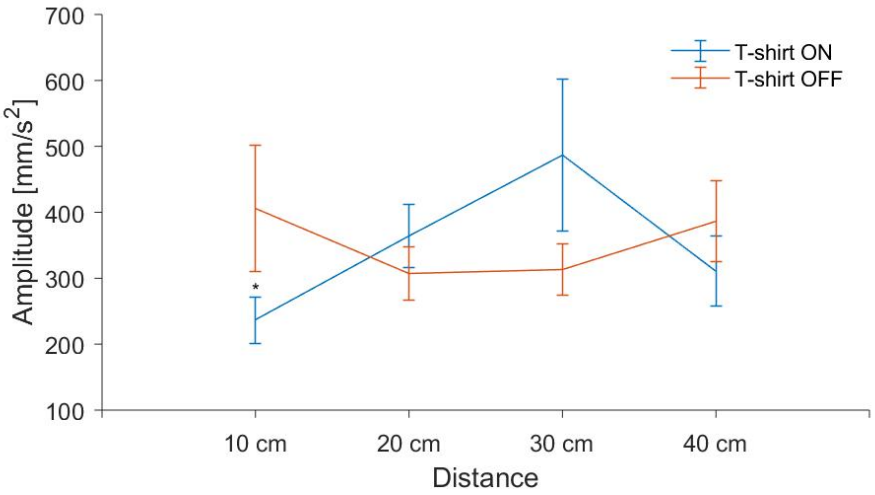

Figure 4.26: Mean peak to peak amplitude for each measurement of the differentiated US signal filtered with *HP86* and *LP25*. T-shirt ON is represented by blue and T-shirt OFF by red. Asterisks indicate significant differences found using post hoc comparison with Bonferroni correction. (* = $p \leq 0.05$).

4.2 Comparison with Accelerometer

One heart beat from each filtered (filters *HP3* and *LP25*) acceleration US signal was subtracted and compared with a heart beat from an accelerometer signal which was filtered in the same way. Three examples of an selected heart beat from the US signal and the accelerometer with different correlation coefficients (best, average, worst) is seen in figure 4.27.

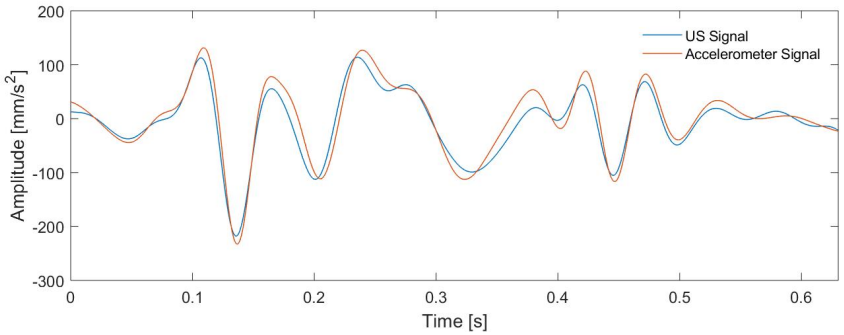

(a) Correlation coefficient 0.969

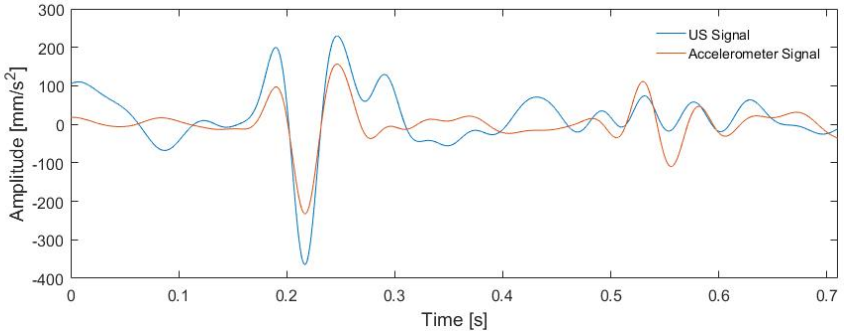

(b) Correlation coefficient 0.760

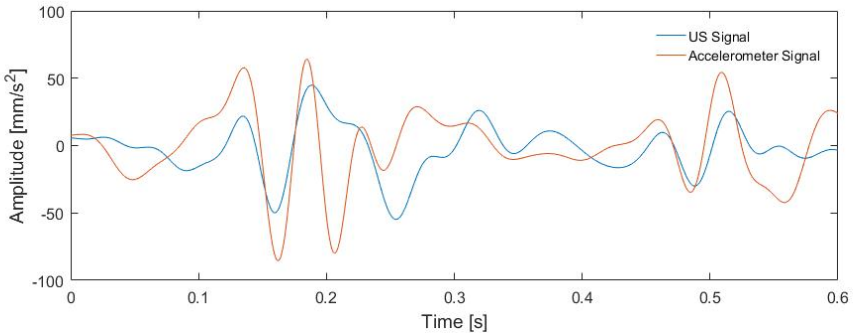

(c) Correlation coefficient 0.386

Figure 4.27: Example heart beat for US signal and accelerometer signal with three different correlation coefficients (best, average, worst).

The correlation between the two extracted heart beats was calculated for each subject. Mean and standard error for the correlation coefficients can be seen in figure 4.28. The best performance was reached with a correlation coefficient of 0.969.

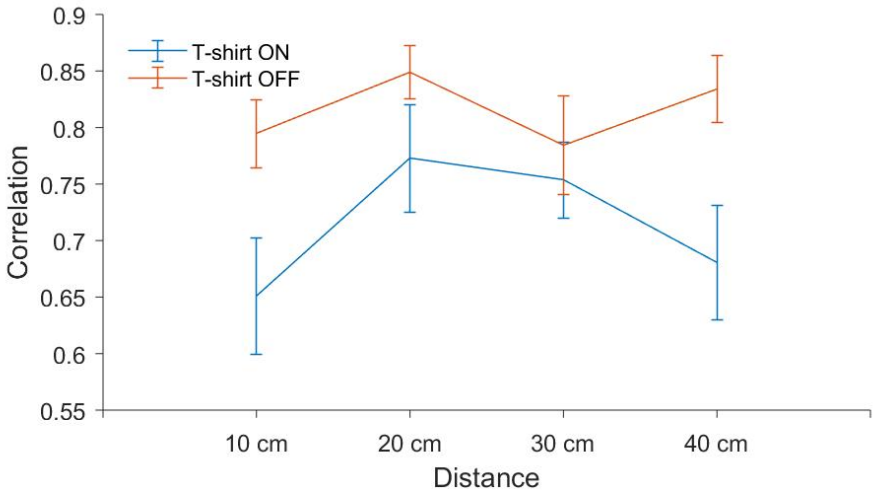

Figure 4.28: Mean peak to peak amplitude for each measurement of the differentiated US signal filtered with *HP86* and *LP25*. T-shirt ON is represented by blue and T-shirt OFF by red.

4.3 Fiducial Points Transposed to Displacement US Signal

A few fiducial points which have been linked to known physiological events (related to heart valves opening and closing) were transposed from the differentiated US signal that had been filtered with *HP3* and *LP25* to the displacement US signal filtered in the same way. This is seen in figure 4.29.

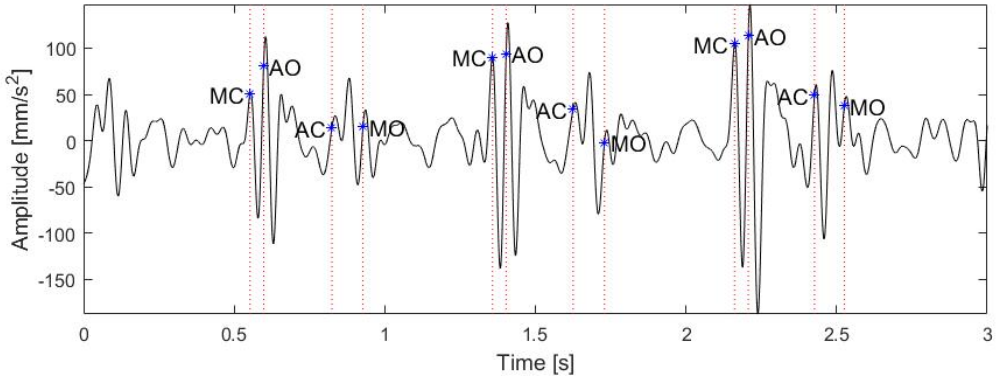

(a) Acceleration US signal

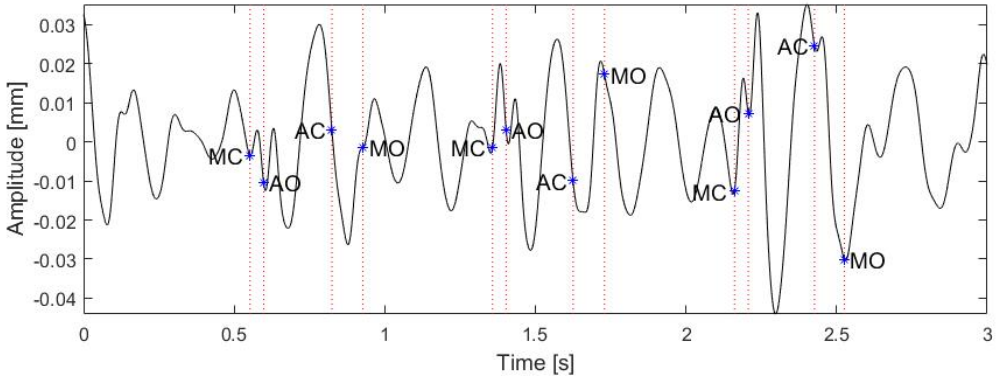

(b) Displacement US signal

Figure 4.29: Four known physiological events located in the displacement US signal. Asterisks indicate the approximate location of the events (Mitral valve closure (MC), aortic valve opening (AO), aortic valve closure (AO), mitral valve opening (MO)).

Part III

Synthesis

Chapter 5

Discussion

Most cardiovascular diseases can be prevented or managed if detected early. Early detection is therefore of great benefit, causing the treatment to be easier, more efficient and economical. Many methods are available for detecting heart disease although most are limited to being contact methods. In this project, a novel method, where the principle of Doppler is utilized for detecting cardiac activity, was examined further. Cardiac signals were recorded using an ultrasound vibrometer and analyzed in terms of different frequency spectra and compared with an accelerometer. This chapter presents a discussion about the experimental setup and signal demodulation, followed by a discussion about the information found in the displacement signal and the comparison with an accelerometer.

Experimental Setup & Signal Demodulation

A subject was seated directly in front of a microphone which was directed at the septum of the subject. A transducer was placed next to the microphone, aiming at the subject at around 20° angle. Multiple ways of setting up the equipment were assessed before this was selected. All included that both the transducer and microphone were directed at the subject. The setups were not experimentally tested, but the signals were visually analyzed by the authors.
The transducer emits at a 30° angle and as the wave reflects of the chest wall in different directions (depending on the angle of reflection) the microphone needed to be in the range of the reflection. The quality of the signal at short distances did not seem to be affected by the setup. However, as the transducer emits at a 30° angle, the area affecting the carrier signal increases as the distance increases. At smaller distances, the area affecting the carrier wave is very small, giving a certain focal point but at larger distances the area affected loses focus. The lack of a focal point seems to introduce some inconsistency in the signal, meaning added noise in the signal and a reduction in the quality of the signal. The reduction of quality can be explained by that the movement of the chest wall differs depending on the location and time points during the respiration cycle [13] and cardiac cycle [15] and therefore when the wave is affected by a larger area, different movements are introduced to the signal, reducing the quality. Furthermore, as the waves are reflected from different locations on the chest, they have different traveling distances and a longer traveling time that affects the phase deviation of the carrier signal. This might lead to demodulation of a phase that is larger than the corresponding displacement of the chest wall, thus giving an incorrect representation of the movement.
This could potentially be fixed with a setup introduced by Jeger-Madiot et al. [32] who designed an elliptical acoustic mirror that reflected the emitted signal, thus obtaining a focal point on the subject and eliminating the uncertainty of the precise origin of the cardiac signal.

A reoccurring and seemingly random problem was found when demodulating the signal where small jumps ($< \pi$) occurred in some of the signals. This is thought to be explained by the carrier frequency and instability in the oscillator. The dominant frequency was calculated from the received signal. It varied between signals and even between parts of the same signal.

The most frequent frequency was 0.2 Hz above the 40 kHz, although the deviation from 40 kHz ranged from being 0.2 Hz below to 0.4 Hz above. This shows that the oscillator is not completely stable and at any given point the carrier frequency is little bit off from the dominant frequency. The dominant frequency was used in the demodulation process thus leaving the system exposed to errors when the oscillator derived from that frequency. The effect this had on the signal is that distortion was introduced to the signal (especially at higher frequencies resulting in high amplitude peaks). This was solved to some degree by splitting the signal into smaller segments to calculate the dominant frequency and demodulate each segment separately. The drawback of doing this is that the demodulated signals were now considerably shorter than the recorded signal. A possible improvement for this would be to monitor the carrier frequency during the recording to have better knowledge about these deviations from the 40 kHz and utilize that knowledge in calculating a more precise carrier wave. Other methods of demodulation are worth considering, e.g. phase lock loop or slope detector, that do not use a local oscillator (used here to obtain the I/Q signals) as such a demodulator might not be as affected by fluctuations in the oscillator as this system is.

Information in different frequency bands

A low frequency signal was extracted (0.1 - 0.5Hz), as this range had most of the energy in the signal (see figure 4.2). Respiration is known to be in this range [14]. The movement of the chest wall due to breathing is larger than the movement due to heart beats (4-12 mm [13] vs 0.2-0.5 mm [15]), and therefore the energy stored in the signal due to breathing overpowers other frequency ranges. DeGroote et al [13] reported the displacement of the chest wall due to breathing in the range of 4-12 mm. This study, however, reports the amplitude a bit lower (overall mean around 3.5 mm, figure 4.4). This might be the effect of a small subject group as this study only had 13 subjects or because of the experimental setup, as subjects were asked not to move during the experiment. Breathing is a voluntary mechanism and was thus very variable between subjects.
Significant difference was found between T-shirt ON and T-shirt OFF at 40 cm distance indicating that clothing influences the signal at this distance. Furthermore, significant difference was found between measurements taken at distance of 40 cm when subject is wearing a T-shirt, compared to other distances. This indicates that at this distance the energy of low frequency factors in the signal is reduced. This could potentially be explained by the system setup as discussed earlier. As the distance is increased the focal point gets lost and the carrier wave is influenced by a larger area which results in a reduced quality of signal.
The energy in frequency spectrum above 0.5 Hz became more visible on the scaleogram after the frequency band related to the breathing had been filtered out, showing high energy in frequencies between 0.6 Hz and 3 Hz (see figure 4.6). Average heart rate during rest in adults ranges from 1 - 1.34 Hz [15], fitting well in the selected frequency range. The overall mean of displacement of the chest wall due to beating of the heart was reported in around 0.3 mm (figure 4.8), which fits well within the range 0.2 - 0.5 mm, reported by Ramachandran et al. [15]. No statistical difference between distances or clothing was found in this frequency range of the signal which indicates that neither distance nor clothing affected the measurement of the displacement.

The magnitude scaleogram of the signal where the heart rate had been filtered out (showing frequencies above 3 Hz) showed that the energy in the signal became more periodic, especially between 8 and 25 Hz. This periodic pattern is interpreted as the systolic and diastolic acoustic waves (corresponding to the valve sounds, S1 and S2). It is difficult to see clear repetitive patterns in the signal in the time domain, although with effort, some repetition

can be observed. The overall mean of the amplitude of the signal that had been band-pass filtered between 3 Hz and 25 Hz was around 3 times less than in the signal showing the heart rate (approximately 0.08 mm, figure 4.11). There was no literature found on displacement of cardiac signal in this frequency range. However, the average amplitude of the acceleration US signal was approximately 340 mm/s^2. According to Rienzo et al [40] a typical seismocardiogram can have an amplitude of a few mg (where 10 mg $\approx$ 100 mm/s^2), although they mention that a seismocardiogram signal can have a frequency range from 0.1 Hz and up to 200 - 300 Hz, which is a larger range than this study explores. The significant difference found in interaction between T-shirt ON/OFF at distance 30 cm might be explained by the reduced quality of the signal at greater distances as mentioned earlier.

Exploring the energy in the signal above 25 Hz showed a clear repetitive pattern between 25 Hz and approximately 90 Hz. The valve sounds could now easily be located in the signal, although some noise was present. Interestingly (and unexpectedly), high energy was observed in a band of rather high frequencies for all subjects although the precise frequency band varied between subjects. We suggest that this could be due the skin's natural resonance frequency. The skin is the last link in transmitting the sound waves from the heart to the surface and acts as an acoustic system. Acoustic systems all have their own natural resonance frequency which should apply here as well. The suggestion is therefore that this occurs at different frequencies for each subject as the skin differs slightly between subjects in terms of e.g. stiffness and elasticity. Silver et al [41] calculated the resonance frequency of decellularized human skin, where he found that the frequency ranged from ca 150 Hz to 350 Hz depending on the strain applied on the tissue. For our subjects this frequency ranged from 190 Hz - 630 Hz with a mean of 335 Hz
The overall mean of the amplitude was decreased by a factor of 10 (was approximately 0.007 mm, figure 4.15) compared to the amplitude of the signal with the frequencies between 3 and 25 Hz. This is considered logical as the effect of the heart valves on the displacement of the chest wall is much smaller than the effect the ventricles have when contracting. The significant difference found in in the amplitude between T-shirt ON/OFF at 10 cm might be explained by a demodulation error that introduces a high peak in the signal that increases the mean amplitude (as discussed earlier).

Analysis of the whole frequency spectrum showed that no noise floor was present in the signal and thus indicating that the bandwidth of the signal could possibly be increased. Subject selective low-pass filtering where the cut-off frequency was below the acoustic resonance frequency band reduced overall noise in the signal and made the heart sounds more visible. As most of the energy seen at these high frequencies was in this band, we suggest that locating and filtering the resonance frequency band with a band-stop filter would allow for an increase in bandwidth of the system.

Wavelet comparison

Differentiating the US signal to obtain the velocity and acceleration is an important step in getting the signal to a comparable form to an accelerometer signal. The downside of differentiating is that it introduces a lot of noise to the signal. However, with some filtering the cardiac activity was retrieved. Distinguishing between systolic and diastolic acoustic waves in lower frequencies (3 - 25 Hz) got easier with each differentiation (see figure 4.20). Valve sounds were detectable for frequencies up to the resonance frequency in the velocity signal, although there was noise present. However, the valve sounds were only detectable in the

acceleration signal when a low-pass filter at 86 Hz was used.

Comparison of the waveforms of the acceleration US signal and the accelerometer signal showed very promising results, with the highest correlation being 0.969 at distance 40cm for T-shirt OFF. The mean correlation coefficient for signals recorded with T-shirt ON was lower than for T-shirt OFF (0.71 and 0.82, respectively) indicating that clothing reduces the quality of the signal. Despite this, cardiac activity was recognizable in all of the signals, for both T-shirt ON/OFF and at all distances. The comparison was carried out by manually selecting one heartbeat complex (including both S1 and S2) from each US signal and the corresponding complex from the accelerometer signal. Therefore, this does not reflect on the overall outcome of the signals but rather the potential this system has in recording cardiac events (i.e. the highest correlation occurring at 40 cm, indicating that a good quality can be reached at higher distances).

Cardiac events (MC, AO, AC and MO) were located on the acceleration US signal (see figure 4.29) corresponding to the definition by Sørensen et al. [39]. After locating the events on the acceleration US signal, the corresponding time points on the US displacement signal were marked. The MC and AO points seemed to always be located in valleys close and adjacent to each other (forming a W pattern) that was followed by a deep valley and a high peak. This pattern could potentially be used in locating these cardiac events. The AC and MO points seemed to be located at more random positions, although AC was always in the downslope of a wave. This process shows the potential for examining the displacement signal further. More cardiac cycle events could easily be transferred to the displacement signal, giving more information about the displacement signal, although this needs a more thorough examination.

As the results present, there is a lot of information on cardiac activity found in the displacement of the chest wall. Due to the information content and ease of execution of the method, it has great potential, both in clinical and out of hospital setting. In order for this method of recording cardiac activity to reach its full potential, additional noise in the signal would need to be reduced. This could be done to some extent by using calculations of a more precise carrier wave and/or designing the hardware in such a way that the wave is directed at the chest wall with a well-defined focal point. Furthermore, recording at closer distances (10 - 20 cm) results in recordings containing less noise than those of far distances.
With these improvements and a suitable hardware design this could be of great benefit in recording of cardiac activity, making the process less time consuming and more convenient for the subject.

Chapter 6

Conclusion

In this project a cardiac signal from 13 subjects was recorded. The signal was recorded using an ultrasound transducer transmitting a 40 kHz ultrasound wave that got frequency modulated when echoing off a subjects chest wall. The US signal was recorded using an ultrasound microphone and processed digitally. It was demodulated using an arctan quadrature demodulator to get the displacement of the chest wall. The displacement US signal was analyzed using continuous wavelet transformation and high and low-pass filters of different cut-off frequencies.

The US displacement signal contains information on different physiological events such as breathing, chamber contraction, and heart valves opening and closing. The effect of distance and clothing was tested and showed that the quality of the signal decreases with increased distance in such a way that the information in the signal due to cardiac activity was harder to detect. Furthermore, recording the signal with a T-shirt on does not reduce the information in the signal.

The correlation of a heart complex from the US acceleration signal and an accelerometer signal was calculated and showed good results with the highest correlation being 0.969. Lastly, physiological events associated with opening and closing of the heart valves were transposed from the acceleration US signal to the displacement US signal.

The displacement signal contains a lot of information on cardiac activity. Due to the information content and ease of execution of this method, it has great potential both in clinical and out of hospital setting. In order to improve this method further, noise in the signal would need to be reduced and the robustness of the system improved. This could be achieved e.g. with improved hardware in terms of getting a focal point on the chest wall, and/or system design in terms of improving stability of the carrier wave and subject specific high frequency noise.

Bibliography

[1] W. H. Organization, "Cardiovascular diseases (CVDs), year = 2017, url = http://www.who.int/news-room/fact-sheets/detail/cardiovascular-diseases-(cvds), urldate = 2018-05-30."

[2] M. Singh and A. Cheema, "Heart Sounds Classification using Feature Extraction of Phonocardiography Signal," *International Journal of Computer Applications*, vol. 77, no. 4, pp. 13–17, 2013.

[3] J. Kranjec, S. Beguš, G. Geršak, and J. Drnovšek, "Non-contact heart rate and heart rate variability measurements: A review," *Biomedical Signal Processing and Control*, vol. 13, no. 1, pp. 102–112, 2014.

[4] J. Kranjec, S. Begus, J. Drnovsek, and G. Gersak, "Novel methods for noncontact heart rate measurement: A feasibility study," *IEEE Transactions on Instrumentation and Measurement*, vol. 63, no. 4, pp. 838–847, 2014.

[5] J. Kranjec, S. Beguš, G. Geršak, M. Šinkovec, J. Drnovšek, and D. Hudoklin, "Design and Clinical Evaluation of a Non-Contact Heart Rate Variability Measuring Device," *Sensors*, vol. 17, no. 12, p. 2637, 2017.

[6] G. J. Tortora and B. Derrickson, *Principles of anatomy and physiology*. John Wiley & Sons, 13th ed., 2012.

[7] M. L. Entman, S. W. Jacob, and M. F. Oliver, "Human Cardiovascular System," *Encyclopædia Britannica*, pp. 1–10, 2014.

[8] "When Your Child Has a Hypoplastic Right Ventricle: Tricuspid Atresia." `https://www.fairview.org/patient-education/89171`. Last accessed: March 2018.

[9] H. Fukuta and W. C. Little, "The Cardiac Cycle and the Physiologic Basis of Left Ventricular Contraction, Ejection, Relaxation, and Filling," *Heart Failure Clinics*, vol. 4, no. 1, pp. 1–11, 2008.

[10] C. Webber and J. P. Zbilut, *InTech Chapter 11 Nonlinear Cardiac Dynamics*. 2012.

[11] D. S. M. Amin and F. Reguig, "Features for Heartbeat Sound Signal Normal and Pathological," *Recent Patents on Computer Science*, vol. 1, pp. 1–8, 2010.

[12] M. Nabih-Ali, E. S. A. El-Dahshan, and A. S. Yahia, "A review of intelligent systems for heart sound signal analysis," *Journal of Medical Engineering and Technology*, vol. 41, no. 7, pp. 553–563, 2017.

[13] A. De Groote, M. Wantier, G. Cheron, M. Estenne, and M. Paiva, "Chest wall motion during tidal breathing," *Journal of Applied Physiology*, vol. 83, no. 5, pp. 1531–1537, 1997.

[14] W. Q. Lindh, M. S. Pooler, C. D. Tamparo, and B. M. Dahl, *Delmar's Comprehensive Medical Assisting Administrative and Clinical Competencies*. fouth ed.

[15] C. Ramachandran and M. Singh, "Three-dimensional reconstruction of cardiac displacement patterns on the chest wall during the P, QRS and T-segments of the ECG by laser speckle inteferometry," *Medical & Biological Engineering & Computing*, vol. 27, no. 5, pp. 525–530, 1989.

[16] G. Shafiq and K. C. Veluvolu, "Surface chest motion decomposition for cardiovascular monitoring," *Scientific Reports*, vol. 4, pp. 1–9, 2014.

[17] A. K. Abbas and R. Bassam, *Phonocardiography Signal Processing*, vol. 4. Morgan & Claypool, 2009.

[18] J. Keroes, L. David, D. Wringley, and B. Erikson, "Heart Murmur," 2017.

[19] L. A. Geddes, "Birth of the stethoscope," *IEEE Engineering in Medicine and Biology Magazine*, vol. 24, no. 1, pp. 84–86, 2005.

[20] A. J. Taylor, *Learning Cardiac Auscultation*. Springer, 2015.

[21] S. Leng, R. S. Tan, K. T. C. Chai, C. Wang, D. Ghista, and L. Zhong, "The electronic stethoscope," *BioMedical Engineering Online*, vol. 14, no. 1, pp. 1–37, 2015.

[22] "Advantages / disadvantages of electronic stethoscopes." `http://www.nursetheory.com/advantages-disadvantages-of-electronic-stethoscopes/`, 2018. (Last accessed: March 2018).

[23] J. M. Zanetti and Salerno, "Seismocardiography: a technique for recording precordial acceleration," *Computer-Based Medical Systems*, pp. 4–9, 1991.

[24] O. T. Inan, P.-f. Migeotte, K.-s. Park, M. Etemadi, K. Tavakolian, R. Casanella, J. Zanetti, J. Tank, I. Funtova, G. K. Prisk, and M. D. Rienzo, "Ballistocardiography and Seismocardiography : A Review of Recent Advances," *Journal of Biomedical and Health Informatics*, vol. 19, no. October, pp. 1414–1427, 2014.

[25] P. Castiglioni, A. Faini, G. Parati, and M. Di Rienzo, "Wearable seismocardiography," *Annual International Conference of the IEEE Engineering in Medicine and Biology - Proceedings*, pp. 3954–3957, 2007.

[26] A. Akhbardeh, K. Tavakolian, V. Gurev, T. Lee, W. New, B. Kaminska, and N. Trayanova, "Comparative analysis of three different modalities for characterization of the seismocardiogram," *Proceedings of the 31st Annual International Conference of the IEEE Engineering in Medicine and Biology Society: Engineering the Future of Biomedicine, EMBC 2009*, pp. 2899–2903, 2009.

[27] A. Dinh, "Heart Activity Monitoring on Smartphone," *International Conference on Biomedical Engineering and Technology*, vol. 11, pp. 45–49, 2011.

[28] J. M. Zanetti and K. Tavakolian, "Seismocardiography : Past , Present and Future," pp. 7004–7007, 2013.

[29] P. Mounsey, "Praicordial ballistocardiography," pp. 259–271, 1956.

[30] R. S. Crow, P. Hannan, D. Jacobs, L. Hedquist, and D. M. Salerno, "Relationship between Seismovardiogram and Echoardiogram for Events in the Cardiac Cycle," *American Journla of noninvasive Cardiology*, vol. 8, pp. 39–46.

[31] P. Shirkovskiy, A. Laurin, D. Chapelle, M. Fink, and R. K. Ing, "Contactless Mapping of Thoracic and Abdominal Motion : Applications for Seismocardiography," *Computing in Cardiology*, 2017.

[32] N. Jeger-Madiot, J. Gateau, M. Fink, and R. Ing, "Non-contact and through-clothing measurement of the heart rate using ultrasound vibrocardiography," *Medical Engineering and Physics*, vol. 50, pp. 96–102, 2017.

[33] S. Haykin, *Communication Systems.* John Wiley & Sons, 2001.

[34] G.Verghese, "Chapter 14: Modulation and demodulation," April 2012.

[35] W. Tranter, K. Shanmugan, T. Rappaport, and K. Kosbar, *Principles of communication systems simulation with wireless applications.* Prentice Hall, 2003.

[36] J. L. Semmlow, *Biosignal and Biomedical Image Processing.* Taylor & Francis Group, third ed., 2014.

[37] A. V. Oppenheim, *Signals and Systems.* Pretnice Hall, 1997.

[38] W. H. Press, W. T. Vetterling, S. A. Teukolsky, and B. P. Flannery, *Numerical Recipes in Fortran 77: The art of scientific computing.* Cambridge University Press, 2 ed., 1992.

[39] K. Sørensen, S. E. Schmidt, A. S. Jensen, P. Søgaard, and J. J. Struijk, "The seismocardiogram in normal subjects," Unpublished.

[40] M. Di Rienzo, E. Vaini, P. Castiglioni, G. Merati, P. Meriggi, G. Parati, A. Faini, and F. Rizzo, "Wearable seismocardiography: Towards a beat-by-beat assessment of cardiac mechanics in ambulant subjects," *Autonomic Neuroscience: Basic and Clinical*, vol. 178, no. 1-2, pp. 50–59, 2013.

[41] F. H. Silver and R. G. Shah, "Analysis of Mechanical Behavior of Composite Tissues Using Vibrational Optical Coherence Tomography," *World Journal of Mechanics*, no. 7, pp. 271–282, 2017.

Appendix A

Carrier Frequency Calculations

The dominant carrier frequency was calculated by Fourier transforming the segment and locating the highest peak in the transformation. Deviation from 40 kHz was calculated. Figure A.1 shows the probability distribution of deviations in the carrier wave for each of the segments (Full signal, middle part, first half and second half) in all of the signals. The carrier frequency most often deviated 0.2 Hz although, there are instances where the deviation becomes $>$ 0.4 Hz and $<$ -0.2 Hz

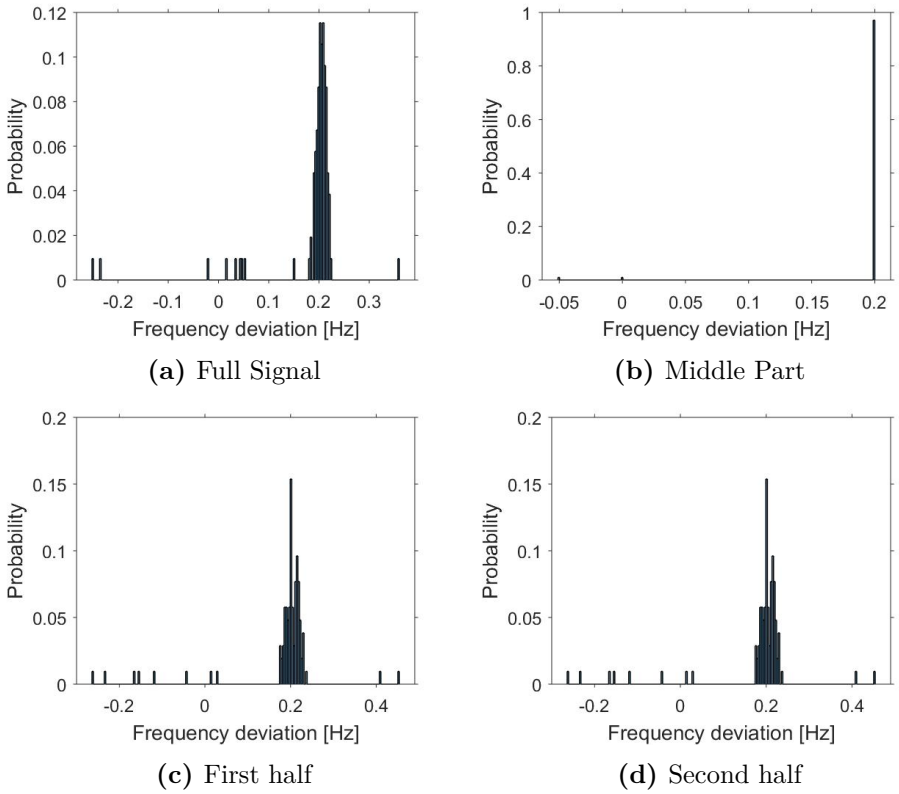

(a) Full Signal **(b)** Middle Part

(c) First half **(d)** Second half

Figure A.1: The histograms show the deviation from the 40 kHz carrier frequency in Hz. **(a)** shows the distribution for the Full signal, **(b)** shows the distribution for the Middle part of the signal and **(c)** and **(d)** show the distribution for the first and second half, respectively.